Neuron

NeuroResource

Comprehensive characterization of metabolic consumption and production by the human brain

Graphical abstract

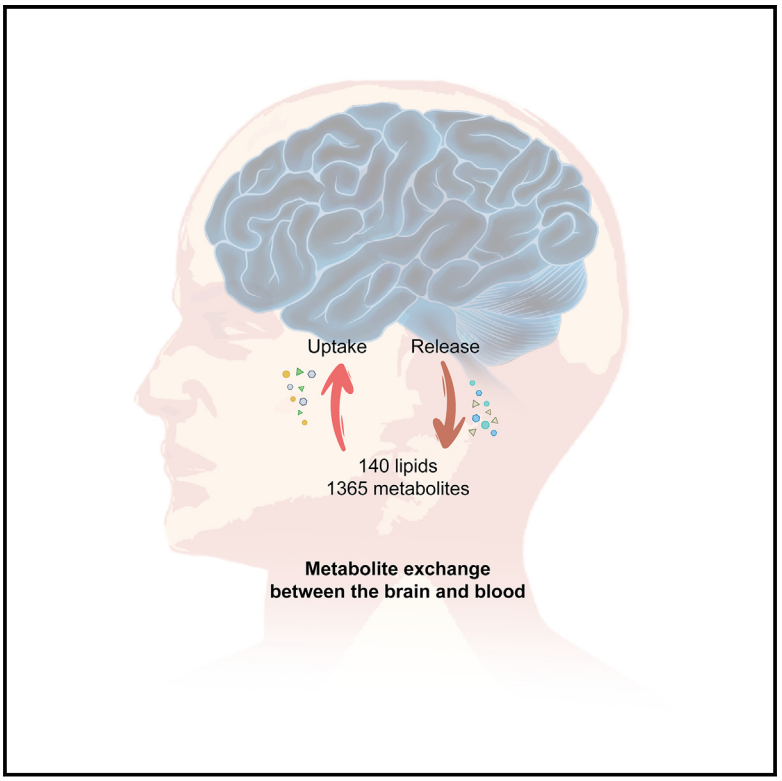

Highlights

- High net uptake of glucose, taurine, and hypoxanthine by the brain
- Glutamine and pyruvate identified as significantly released by the brain
- Triacylglycerols are the most prominent lipids consumed by the brain
- Metabolic differences between CVSS and CVST brains, along with age-related alterations

Authors

Yilong Wang, Lebo Zhou, Nan Wang, ..., Zhen Li, Dapeng Mo, Woo-ping Ge

Correspondence

yilong528@aliyun.com (Y.W.),
bjttmodp@163.com (D.M.),
woopingge@cibr.ac.cn (W.-p.G.)

In brief

Wang et al. profile the brain's metabolic uptake and release by comparing blood samples from the cerebral venous sinus and femoral artery. The study identifies key metabolites and lipids consumed or released by the brain. It also highlights age-related changes in metabolic processes.

Wang et al., 2025, Neuron *113*, 1708–1722
June 4, 2025
https://doi.org/10.1016/j.neuron.2025.03.003

CellPress

CellPress
OPEN ACCESS

Neuron

NeuroResource

Comprehensive characterization of metabolic consumption and production by the human brain

Yilong Wang,[1,2,3,13,*] Lebo Zhou,[1,2,4,13] Nan Wang,[1,2,13] Baoshan Qiu,[1,2,13] Di Yao,[2,4] Jie Yu,[2,4,5] Miaoqing He,[2,4,6] Tong Li,[2,4] Yufeng Xie,[2,4,7,8] Xiaoqian Yu,[2,4] Zhanying Bi,[2,4,9] Xiangli Sun,[2,4] Xunming Ji,[10] Zhen Li,[2,4] Dapeng Mo,[1,11,*] and Woo-ping Ge[2,4,8,12,14,*]

[1]Department of Neurology, Beijing Tiantan Hospital, School of Basic Medical Sciences, Capital Medical University, Beijing 100070, China
[2]Chinese Institute for Brain Research, Beijing, Beijing 102206, China
[3]China National Clinical Research Center for Neurological Diseases, National Center for Neurological Disorders, Beijing 100070, China
[4]Beijing Institute for Brain Research, Chinese Academy of Medical Sciences & Peking Union Medical College, Beijing 102206, China
[5]Department of Neurology, First Affiliated Hospital, School of Medicine, Zhejiang University, Hangzhou 310003, China
[6]Academy for Advanced Interdisciplinary Studies (AAIS), Peking University, Beijing 100871, China
[7]Department of Biochemistry and Molecular Biology, Peking Union Medical College, Beijing 100730, China
[8]Changping Laboratory, Beijing 102206, China
[9]College of Life Sciences, Nankai University, Tianjin 300071, China
[10]Department of Neurology, Xuanwu Hospital, Capital Medical University, Beijing, China
[11]Department of Interventional Neuroradiology, Beijing Tiantan Hospital, Capital Medical University, Beijing 100070, China
[12]Department of Neurosurgery, Xuanwu Hospital, Capital Medical University, Beijing 100053, China
[13]These authors contributed equally
[14]Lead contact
*Correspondence: yilong528@aliyun.com (Y.W.), bjttmodp@163.com (D.M.), woopingge@cibr.ac.cn (W.-p.G.)
https://doi.org/10.1016/j.neuron.2025.03.003

SUMMARY

Metabolism is vital for brain function. However, a systematic investigation to understand the metabolic exchange between the human brain and circulatory system has been lacking. Here, we compared metabolomes and lipidomes of blood samples from the cerebral venous sinus and femoral artery to profile the brain's uptake and release of metabolites and lipids (1,365 metabolites and 140 lipids). We observed a high net uptake of glucose, taurine, and hypoxanthine and identified glutamine and pyruvate as significantly released metabolites by the brain. Triacylglycerols are the most prominent class of lipid consumed by the brain. The brain with cerebral venous sinus stenosis (CVSS) consumed more glucose and lactate and released more glucose metabolism byproducts than the brain with cerebral venous sinus thrombosis (CVST). Our data also showed age-related alterations in the uptake and release of metabolites. These results provide a comprehensive view of metabolic consumption and production processes within the human brain.

INTRODUCTION

The mammalian brain is characterized by its substantial energy demands and distinctive metabolic activities. Despite its relatively small size (~2% of body weight), the human brain consumes nearly 20% of the body's glucose and oxygen resources.[1–3] This underscores the crucial role of various biochemical components, such as energy-supplying fuels, amino acids, and lipids, in supporting essential processes such as brain growth, development, aging, neural activity initiation, and propagation, as well as the maintenance of brain homeostasis.[4,5]

The exchange of metabolites and lipids between the brain and the circulatory system plays a pivotal role in delivering vital fuels and nutrients to the brain while efficiently removing metabolic byproducts and waste materials.[6–8] The comparison of arteriovenous differences has long been used as a fundamental method for investigating tissue metabolism by assessing substance quantities across tissues.[9–13] In particular, glucose is recognized as the primary energy source for the mammalian brain.[14] Early studies in dogs[15] and humans[16] demonstrated that the brain uses glucose at a net rate exceeding 10% on the basis of arteriovenous glucose comparisons. Although other metabolites are known to be exchanged across the brain, including lactate, pyruvate, glutamate, and glutamine,[17–19] the uptake and release patterns of most metabolites in the brain remain largely unknown.

Metabolomic measurement facilitates high-throughput and comprehensive characterization of small-molecule chemicals in organs, tissues, cells, and biofluids.[20] To date, over 20,000 metabolites have been detected in human blood serum (Human Metabolome Database, HMDB; https://hmdb.ca/). Recent

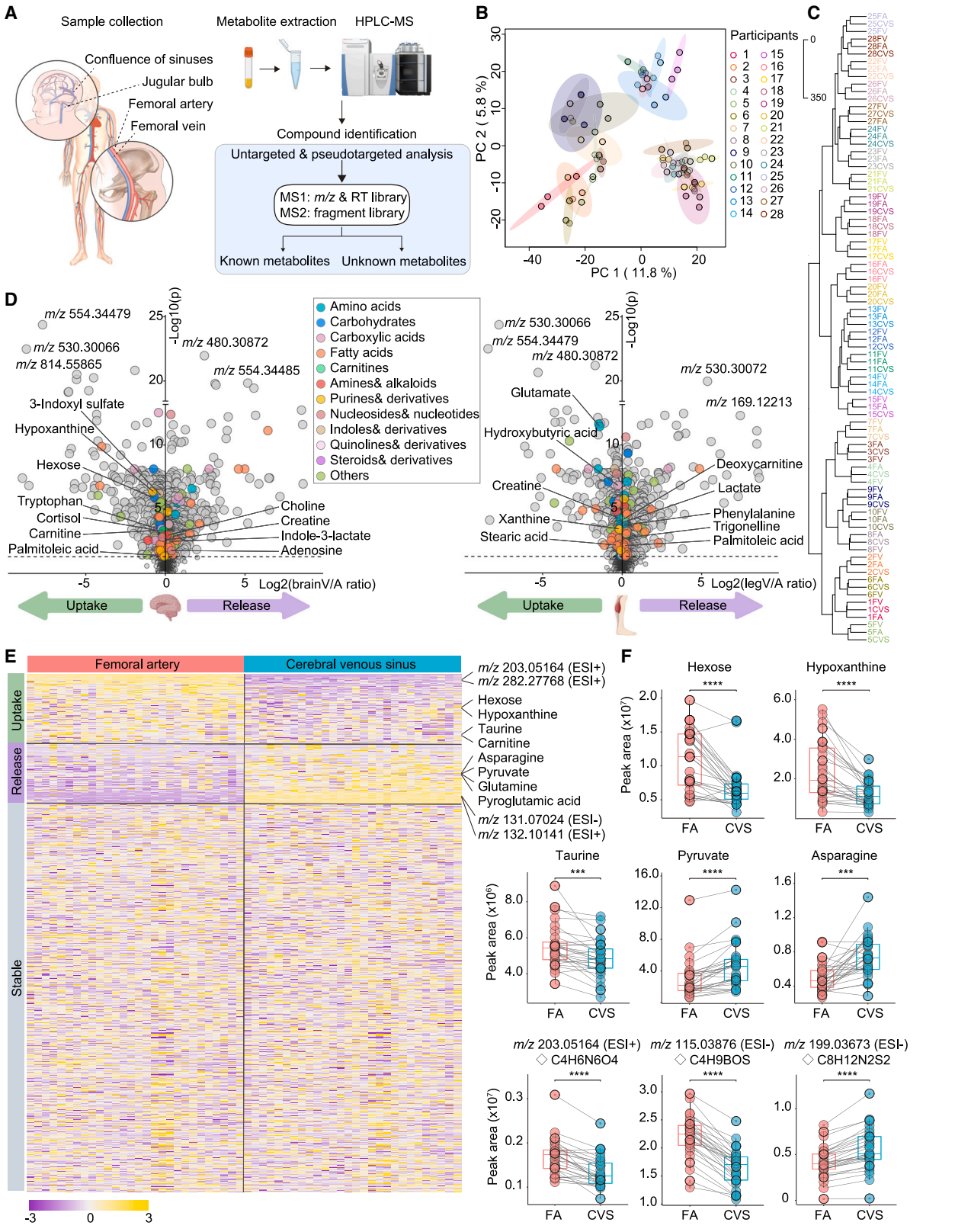

(legend on next page)

advances in metabolomics have led to the application of arteriovenous metabolomics in pigs[10] and brain tumors,[11] allowing for the quantification of organ-specific or tissue-specific metabolite exchange. This approach has provided insights into fuel utilization in the human heart.[9] Profiling the uptake and release of substances by the brain can provide a valuable reservoir of metabolite and lipid information, laying a solid foundation for improving brain health and understanding brain metabolism in disease contexts. Therefore, there is an urgent need within the brain research community to investigate the exchange of metabolites between the human brain and the bloodstream in a high-throughput manner. In this study, we used untargeted metabolomic methods and targeted lipidomic analysis to comprehensively characterize the metabolic or lipid consumption and production by the human brain.

RESULTS

Metabolomic profiling of blood samples for brain arteriovenous analysis

To investigate the metabolic uptake and release by the human brain, we conducted a non-targeted metabolomic analysis of blood samples collected from arteriovenous sites. Our study included 28 subjects (9 males, 19 females) with an average age of 35.9 ± 11.1 years who were undergoing cerebral venous interventional surgery (Table S1).

Arterial blood samples were collected from the femoral artery (FA). Venous blood samples were collected from the jugular bulb, or venous sinus, or confluence of sinuses (collectively called the cerebral venous sinus, CVS) for the brain arteriovenous analysis. Peripheral venous blood samples were collected from the femoral vein (FV) for the leg analysis. We performed global metabolomic profiling on these samples (Table S2). Then, we calculated the ratio of metabolite abundance in the vein (V) relative to the artery (A). Ratios (V/A) < 1 indicated net uptake, whereas ratios > 1 indicated net release (Figure 1A).

The global metabolite profiles of the three plasma samples (the FV, FA, and CVS samples) from these subjects closely aggregated in a principal-component analysis (PCA, Figure 1B). An unsupervised clustering analysis also showed that the three samples from each subject clustered together, whereas the distances between individuals were substantially greater than the arteriovenous differences within a subject (Figure 1C). This finding suggests good biological reproducibility of the dataset and a larger metabolic distinction among individuals as compared with the arteriovenous differences within the same subject.

The comparison of arteriovenous metabolomes from the brain (b-CARVE)

To comprehensively cover the human plasma metabolome, 5,384 ion features were measured after we performed global untargeted metabolomics analysis. Among these compounds, we identified 1,365 metabolites that were taken up by or released from the human brain (Figure 2A).

The metabolites taken up by or released from the brain exhibited a diverse range of general classes. For most of the annotated metabolites (55 of 76 metabolites), the net uptake/release, the absolute value of (V–A)/A, was <30% (A, V, the relative abundance of a metabolite in FA or CVS samples; Figures 1D and S1; Table S2), although some unidentified compounds showed a larger net uptake/release. Of the 5,384 compounds analyzed, 738 (13.7% of all features measured) were taken up by the brain, 627 (11.6%) were released from the brain, and the remaining 74.7% remained stable, showing no significant difference in value between arterial and venous plasma samples (Figure 1E).

The data revealed that hexose, which is found primarily as D-glucose in human blood, was taken up by the human brain (Figures 1D and 1F). Additionally, the principal purine in blood plasma, hypoxanthine, was taken up by the human brain at a net amount of 42% (Figures 1D and 1F), confirming previous research suggesting that plasma hypoxanthine and/or inosine serve as a definite source of purines for the brain.[21] Furthermore, taurine was significantly taken up by the brain (Figure 1F). The human brain also released pyruvate and asparagine into the venous blood (Figure 1F), as well as choline, creatine, and adenosine (Figure 1D), whereas tryptophan, cortisol, and carnitine were taken up by the brain. We observed that the uptake of many hydrophilic metabolites (i.e., hexose, glutamate, lactate, hypoxanthine, and cystine) was directly proportional to circulating levels in the brain, indicating that the consumption of these nutrients was driven by substrate availability (Figures S2A–S2F). The release of glutamine, pyruvate, and asparagine from the brain also correlated with their circulation in abundance (Figures S2G–S2I). Moreover, our metabolomic data demonstrated a large number of unannotated metabolites that were taken up by and released from the human brain. For instance, a substance with a predictive formula C4H9BOS was taken up by the brain at a net value of 26% (Figure 1F).

Untargeted arteriovenous analysis of metabolic exchange across the leg

The metabolic exchange across the human leg was used as a control organ for the brain. Our comparison of metabolite

Figure 1. Profiling metabolic exchange between blood and the human brain

(A) Experimental design and workflow schematic. MS1, MS2, two mass spectrometers in tandem. RT, retention time, *m/z*, mass-to-charge ratio.

(B) Principal-component analysis (PCA) of untargeted metabolomic data from plasma samples of 28 participants.

(C) Hierarchical clustering dendrogram of plasma samples from the femoral artery (FA), cerebral venous sinus (CVS), and femoral vein (FV) of 28 participants.

(D) Volcano plots illustrating substances taken up by and released from the human brain (left) and leg (right). Significance was determined using two-tailed paired t test or one-sample Wilcoxon test. Dashed line represents $p = 0.05$.

(E) Heatmap showing relative abundance of detected compounds in plasma of the FA versus CVS for 28 participants. Scale bar indicates relative abundance.

(F) Representative metabolites and features taken up by and released from the human brain. Scatterplots display peak areas of metabolites and features in corresponding samples, with lines connecting samples from the same individual. Boxplots depict median and lower and upper quartiles. Significance was determined using Benjamini-Hochberg-corrected *p* values after a two-tailed paired t test or one-sample Wilcoxon test. ◇ denotes predictive chemical formulas. ***$p < 0.001$, ****$p < 0.0001$.

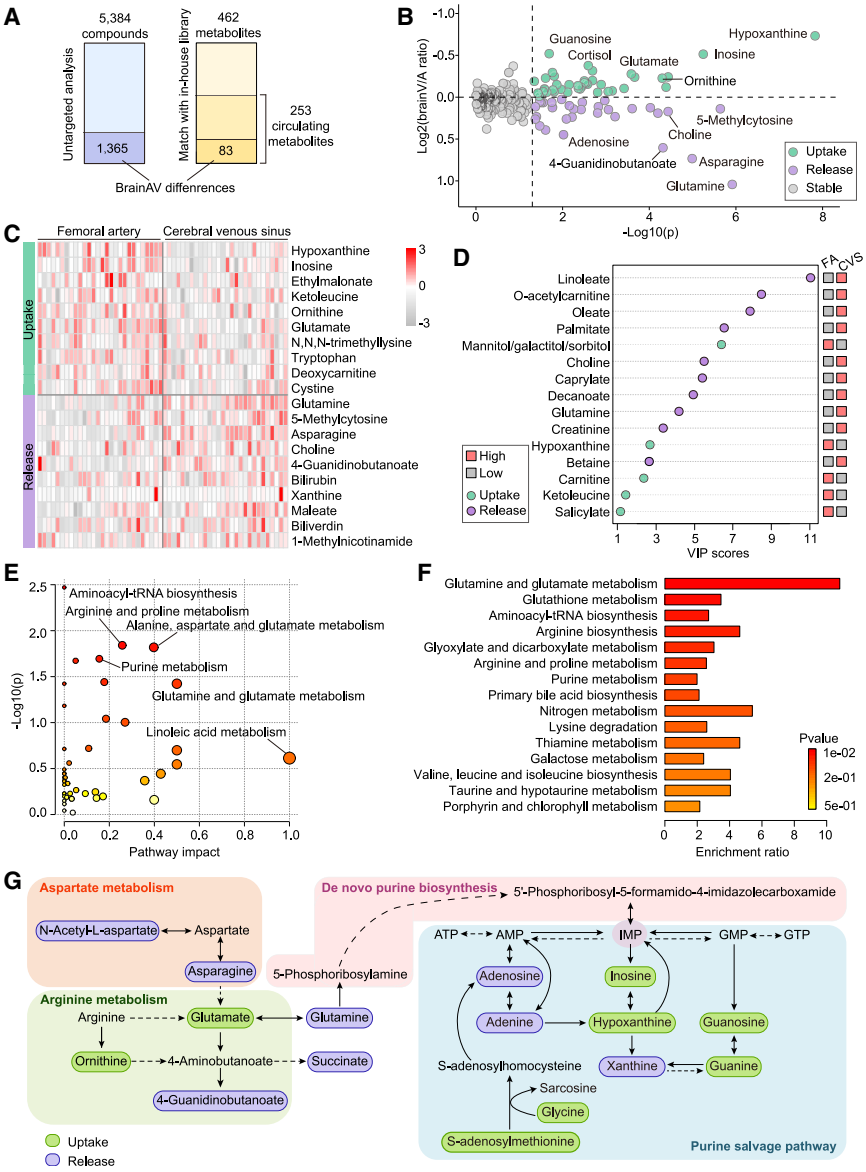

Figure 2. Metabolomics analysis and pathway identification with an in-house library

(A) Total identified compounds and those showing significant arteriovenous (A-V) differences in the human brain through untargeted analysis (left). Total metabolites, circulating metabolites, and metabolites exhibiting significant A-V differences in our in-house library (right). Significance was determined using Benjamini-Hochberg-corrected p values after a two-tailed paired t test or one-sample Wilcoxon test.

(B) Volcano plot illustrating circulating metabolites matched with our in-house library. Significant A-V differences in the brain were determined using two-tailed paired t tests or one-sample Wilcoxon tests. The vertical dashed line indicates $p = 0.05$, and the horizontal dashed line indicates no A-V difference, i.e., $\log_2$(brain V/A) = 0.

(C) Top 20 metabolites (ranked by p values from the brain A-V; two-tailed paired t test or one-sample Wilcoxon test) that differ significantly between the FA and CVS. Colorimetric representation of relative abundance in each sample is presented according to the scale bar.

(D) Variable importance in projection (VIP) scores for metabolites between FA and CVS. Fifteen metabolites with VIP scores > 1, which thus contribute maximally to group classification, are shown. Squares on the right indicate the relative abundance of each metabolite in each plasma group.

(E) Pathway analysis for metabolites exhibiting significant brain A-V differences ($p < 0.05$).

(F) Metabolite set enrichment analysis (MSEA) for metabolites taken up by the human brain, showing enriched pathways ranked by their corresponding p-values.

(G) Summary diagram of representative pathways related to glutamate, glutamine, aspartate, arginine, and purine metabolism in relation to (E). The solid line and dashed line indicate whether the reaction occurs in a single step or multiple steps, respectively.

abundance in FA and FV showed a statistically significant uptake or release of 1,508 compounds across the leg (Figures 1D and S3A). Consistent with its crucial role in providing energy for muscle function, hexose was taken up by the leg, with a median ratio of 31% (Figure S3B). Additionally, glutamate, a key neurotransmitter in the central nervous system, was significantly taken up by the leg (Figure S3C). By contrast, lactate was released from the leg at a ratio of 10.3% (Figure S3G; Table S2). Moreover, other metabolites such as hydroxybutyric acid (Figure S3D), creatine (Figure S3E), and xanthine (Figure S3F) were taken up by the leg, while creatinine (Figure S3H) and deoxycarnitine (Figure S3I) were notably released from the leg. Compared with the brain, the leg showed a similar glucose uptake but released less of the sugar metabolism product pyruvate (Figure S3J). The leg released the anaerobic respiration product lactate, whereas the brain took it up (Figure S3J). The leg took up the ketone body, β-hydroxybutyric acid, whereas the brain released it (Figure S3J). The brain and leg also differed in the exchange properties of many other metabolites, including glutamate, asparagine, deoxycarnitine, tyrosine, etc. (Figure S3K). The metabolic pathways enriched by the arteriovenous differential metabolites of the leg show many differences from those observed in the brain. The key metabolic pathways in the legs are closely related to energy metabolism, including glucose metabolism, various amino acid metabolism pathways, and lipolysis (Figures S3L and S3M).

We further developed an in-house library consisting of 462 authenticated chemical standards of canonical pathway metabolites. With this library, we identified 253 metabolites with reliable confirmation of their identities. A differential analysis of the abundance of these metabolites between the CVS and FA showed that 82 metabolites were significantly altered across the brain (Figures 2A and 2B). Among them, 18.2% (46 of 253) of the

metabolites were taken up by the brain, whereas 14.6% (37 of 253) were released from the brain to the circulation system (Figure 2B). Notably, these metabolites, including hexose, hypoxanthine, cortisol, and glutamate, showed consistent patterns in both the metabolomic analysis using the in-house library and the untargeted data.

We used the general pattern analysis and differential analysis to identify the five metabolites that were most significantly and extensively taken up by the brain: hypoxanthine, inosine, cortisol, cortisone, and glutamate (Figure 2C). Additionally, we identified the five most significantly released metabolites as glutamine, asparagine, 4-guanidinobutanoate, adenosine, and deoxyguanosine (Figure 2C). To determine which metabolites dominated the separation between the FA and CVS groups, we further conducted a partial least-squares discriminant analysis (PLS-DA). The nine metabolites that had the greatest effect on differentiating the blood in the FA from that in the CVS were linoleate, *O*-acetylcarnitine, hexitol, choline, caprylate, decanoate, glutamine, creatinine, and hypoxanthine (Figure 2D).

To gain a deeper understanding of the pathways that are enriched at the organ level, we conducted pathway analyses for all metabolites taken up by and released from the brain. Several significant pathways involved the influx and/or efflux of metabolites, such as aminoacyl-tRNA biosynthesis; arginine and proline metabolism; alanine, aspartate, and glutamate metabolism; glutamine and glutamate metabolism; and purine metabolism (Figure 2E).

To further investigate the prominent pathways influenced by the metabolites absorbed into the brain, we performed metabolite set enrichment analysis (MSEA). The top 15 enriched pathways were identified, which included glutamine and glutamate metabolism, glutathione metabolism, and purine metabolism (Figure 2F). These results indicate the importance of glutamate and glutamine metabolism as a central pathway, while also emphasizing the intricate interplay between various metabolic processes involving amino acids, nucleosides, and nucleotides in the brain.

Subsequently, our focus turned to an in-depth analysis of several key pathways, specifically (1) the glutamine and glutamate pathways due to their crucial role in neuromodulatory activities,[1,2] (2) amino acid pathways enriched with aspartate and arginine as representative compounds in our study, and (3) purine metabolism, which includes both the *de novo* purine biosynthesis (DNPB) pathway and the purine salvage pathway (PSP), encompassing multiple metabolite members that ranked high in our differential analysis (Figures 2B and 2C) and variable importance in projection (VIP) plot (Figure 2D).

In the integrated view (Figure 2G), we observed that glutamate (15.3%, taken up) was connected to aspartate metabolism (*N*-acetyl-L-aspartate, 4.3%, released and asparagine, 66.3%, released) and arginine metabolism (ornithine, 14.5%, taken up, and 4-guanidinobutanoate, 52.0%, released). Additionally, glutamate can be converted into glutamine (106.0%, released), which may be involved in the DNPB pathway. Notably, the PSP was enriched for multiple metabolites that are taken up by the brain (such as hypoxanthine, inosine, guanosine, guanine, glycine, and *S*-adenosylmethionine) and metabolites that are released from the brain (including adenosine, adenine, and xanthine) (Figure 2G).

Previous research has suggested that the brain has limited capacity for *de novo* purine and pyrimidine synthesis and often relies on nucleosides and nucleotides synthesized *de novo* in the liver.[22] Interestingly, our data indicated that the PSP—which represents relatively rapid and energetically frugal processes that can swiftly increase neuronal activity, particularly during stress situations when substrate availability is elevated[23]—was notably active in the human brain relative to the DNPB pathway. This finding is consistent with recent transcriptomic evidence, which indicates that the PSP dominates in brain tissue rather than the DNPB pathway.[23,24] These results, therefore, suggest that the human brain salvages preformed purines from the blood while simultaneously using liver-derived nucleosides.

Validation of glutamate uptake through stable isotope tracing

We performed isotope tracing experiments with jugular vein catheterization in mice to verify whether these metabolites truly enter the brain parenchyma. After [U^{13}C] glutamate infusion started, the C13 labeling of glutamate and glutamine in blood gradually reached a steady state (Figure S4A). As a major neurotransmitter, the concentration of glutamate in the brain was significantly higher than in the thigh muscle (Figure S4B). Our data validated that circulating glutamate entered the brain and revealed circulating glutamate as a contributor to the carbon sources of glutamate in the brain and thigh muscle (Figure S4C).

Quantification of the metabolic demand and production of the human brain

To precisely determine the uptake and production of various metabolites by the human brain, we calculated the net amount of each metabolite that was taken up or released in terms of micromoles per liter of blood flowing through the brain (Figure 3). For metabolites present in our library, we used external standard determination, whereas publicly reported concentrations from the HMDB were used for the remaining ones.

We observed glucose was taken up by the brain at 15.9%, with a net uptake of 656.47 μM (Figure 3A). Lactate, considered an energy source and signaling molecule for the brain, showed a net uptake of 130.67 μM (8.8%, Figure 3A). Glutamate demonstrated a net uptake of 29.98 μM, whereas glutamine, another amino acid, was the metabolite that was released in the greatest amount (439.18 μM), far exceeding the molar amount of absorbed glutamate (Figure 3B). This suggests that released glutamine may have been formed from excess glutamate in the brain and recycled ammonia. We observed significant arteriovenous differences in glutamine levels (439.18 μM), which are higher than the values reported in previous studies on brain glutamine exchange in head trauma patients (release of 27–49 μM)[19] and in young subjects (release of 13–25 μM) and older subjects (61–62 μM).[12,25,26] This discrepancy may stem from differences in collection and subject conditions, such as sampling location or anesthesia. Notably, our findings reveal a higher release of glutamine by the brain, with potential sources including glucose, lactate, and 3-methylglutaconate (3MGA). The arteriovenous differences for glucose, lactate, and 3MGA in our data were 656.47, 130.67, and 116.33 μM, respectively. These results suggest that the extent of glutamine release from the brain is comparable to other metabolites that may contribute to its production. By contrast, γ-aminobutyric acid (GABA) did not show a net

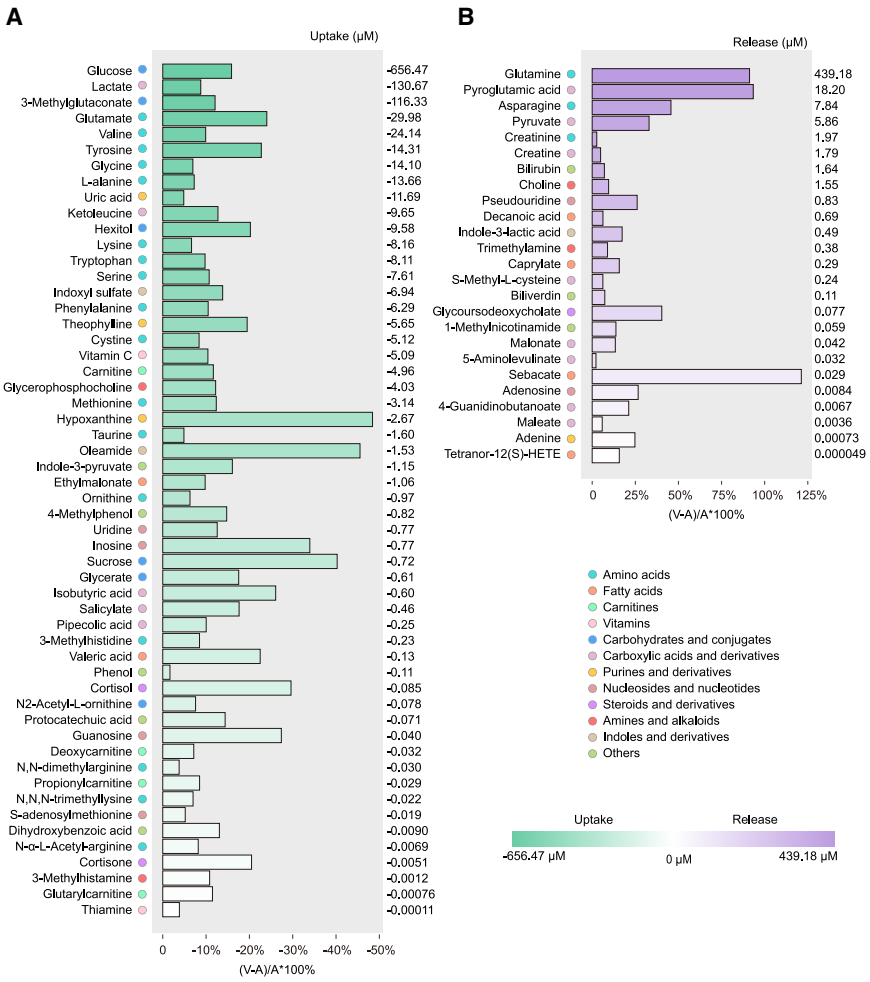

Figure 3. Metabolite uptake and release by the human brain

The net uptake (A) and release (B) in micromoles per liter of blood flowing through the brain and the ratios of metabolites consumed by the human brain. Bar colors denote metabolite uptake or release, whereas the intensity of the shading reflects the absolute quantities of net absorption or release. The lengths of the bars represent the uptake (A) or release (B) ratios of the corresponding metabolites. Dots of varying colors represent metabolite classifications.

exchange across the brain. Many amino acids were taken up by the brain in larger amounts, most of which were >1 μM. Aromatic amino acids (tyrosine, tryptophan, and phenylalanine), precursors of monoamine neurotransmitters (serotonin, dopamine, and norepinephrine),[27] each had a net uptake by the adult brain at 6 to 15 μM. Only a few amino acids (glutamine, asparagine, and creatine) were released by the brain, and no essential amino acids were released, indicating minimal protein hydrolysis activity in the human brain, unlike the active proteolysis that occurs in the human heart.[9]

The metabolite hypoxanthine demonstrated the largest net uptake (48.4%) by the brain. Among nucleosides and nucleotides, inosine, guanosine, uridine, and *S*-adenosylmethionine were taken up by the brain, whereas pseudouridine and adenosine were released from the brain. The brain also gained hormones (cortisol, cortisone, and testosterone sulfate) and vitamins, including vitamin C (VC) and thiamine, from the circulation (Figure 3A). Notably, our data identified indoxyl sulfate, a microbiota–host co-metabolite derived from the common amino acid tryptophan,[28] to be significantly absorbed by the human brain at 6.94 μM. This finding supports the existence of a gut-microbiota-brain connection in humans, in which microbiota-derived metabolites may cross the blood-brain barrier and reach the central nervous system.[29,30]

Quantification of the lipids consumed and released by the human brain

To determine the lipids taken up or produced by the human brain, we conducted targeted lipidomics measurement, quantifying arterial and venous concentrations of 654 lipids. PCA revealed close clustering of the three plasma samples from the same subject among the 28 individuals (Figure 4A). Across the 27 lipid classes measured (Figure 4B), we observed overarching trends of lipid exchange in the human brain (Figure 4C) and leg (Figure S5A). The brain took up 63 lipids, including triacylglycerol (TAG)54:8(22:6), phosphatidylcholine (PC)36:4(18:2_18:2), sphingomyelin (SM) d18:0/16:0, sphingosine-1-phosphate (S1P) d18:1, etc., and released 77 lipids, including phosphatidylethanolamine (PE)38:6, phosphatidylinositol (PI)38:4(18:0_20:4), free fatty acid (FFA)20:5, lyso-PC (LPC) 18:2, diacylglycerol (DAG)34:1(16:0/18:1), lyso-PI (LPI)20:4, lyso-PE (LPE)18:1, etc. (Figures 4D and 4F). The predominant lipids absorbed by the brain were triacylglycerols (TAG) (52/63, 82.5%) (Figure 4E). PE (23/77, 29.9%), PI (10/77, 13.0%), and FFA (9/77, 11.7%) were the top three prominent lipid classes released by the brain (Figure 4F). By contrast, the leg took up 35 lipids, including ceramide (Cer), phosphatidylglycerols (PG), sulfatides (SL), and TAG (Figures S5B and S5C), and released 30 lipids, including TAG, PI, PC, LPC, carnitine, DAG, cholesteryl ester (CE), and FFA (Figures S5B and S5D). Similar to the brain, most of the lipids absorbed by the leg were TAG (28/35, 80.0%) (Figure S5C). FFA (13/30, 43.3%) and CE (7/30, 23.3%) showed remarkable release nature by the leg (Figure S5D).

We computed the net demand and production of these lipids, measured in nano/micromoles per liter of blood passing through the brain (Figure 5; Table S2) or the leg (Figures S5E and S5F; Table S2). TAG50:3(18:2) was the most consumed lipid by the brain, at 587.62 nM, followed by TAG52:4(16:1) at 557.44 nM (Figure 5A). TAG48:4(16:1) and TAG46:2(16:0) showed the highest net uptake ratios, accounting for 21.1% and 18.2%, respectively (Figure 5A). Total FFA was net

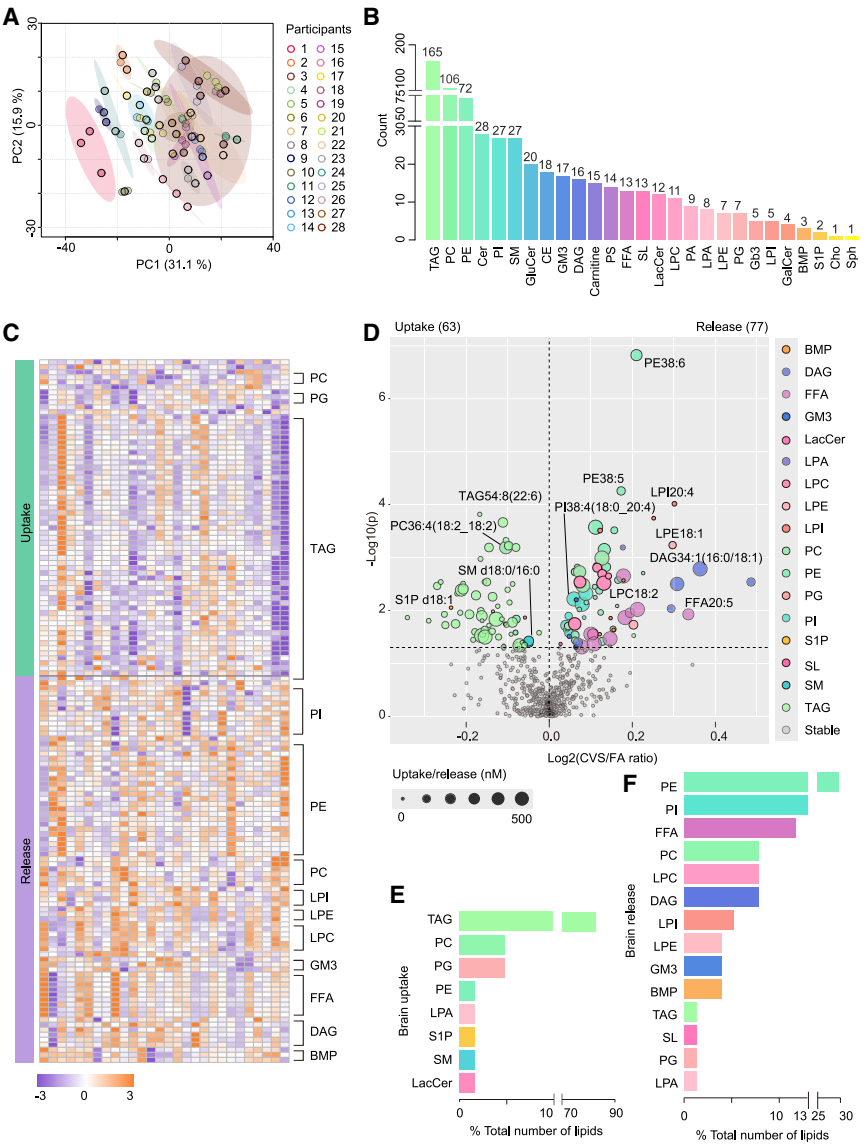

Figure 4. The landscape of lipids consumed and released by the human brain

(A) PCA plot of lipidomics data from plasma samples of 28 participants.

(B) Class composition and number of lipids detected in the plasma samples. "Count" refers to the number of lipids detected in the respective category.

(C) Heatmap showing differences of lipid abundance in CVS versus FA. Scale bar indicates relative lipid differences in CVS versus FA.

(D) Volcano plot showing lipids taken up by and released from the human brain. Significant FA-CVS differences in the brain were determined using two-tailed paired t tests or one-sample Wilcoxon tests. The vertical dashed line indicates $p = 0.05$, and the horizontal dashed line indicates no A-V difference, i.e., $\log_2$(CVS/FA) = 0.

(E and F) Class composition of lipids taken up (E) or released by (F) by the brain. Number of lipids in each lipid class as a percentage of the total number of lipids taken up or released by the brain.

produced and released into the blood at 145.44 μM (Figure 5B). FFA18:2 and FFA18:3 were the 1st and 2nd highest lipids released by the brain, with net values of 46.38 and 8.58 μM, respectively (Figure 5B). DAG32:1(16:1/16:0) displayed the largest net release ratio (40.0%), with DAG34:1(16:0/18:1) ranking second (28.6%) (Figure 5B). While TAG and FFA have previously been reported to cross the blood-brain barrier (BBB),[31,32] our results identify many lipids whose exchange dynamics and functional roles in the brain remain insufficiently explored.

In the leg, TAG54:5(18:2) and TAG54:5(18:1) were the most absorbed lipids, at 828.57 and 588.55 nM, respectively (Figure S5E). TAG58:7(20:4) (9.71%), TAG56:5(18:2) (9.50%), and Cer d18:1/22:0 (9.25%) were the lipids net absorbed by the leg with the highest ratios (Figure S5E). CE18:2 (471.23 μM) and FFA (251.05 μM) were the most released lipids from the leg (Figure S5F). FFAs, especially FFA18:3 (34.3%), FFA16:1 (32.8%), and FFA18:4 (28.5%), exhibited the highest release ratios from the leg (Figure S5F).

To investigate the characteristics and physiological effects of lipids absorbed or released by the brain, we conducted lipid ontology (LION) enrichment and network analysis.[33] The majority of lipids absorbed by the brain had neutrally charged head groups, particularly glycerolipids. These lipids were primarily associated with lipid storage, and the absorbed lipids could contribute to the formation of lipid droplets in cellular components (Figures S6A and S6B). The lipids released into circulation by the brain were mainly linked to raw materials required for forming cellular membrane components, endoplasmic reticulum, or mitochondria (Figure S6A).

Age-dependent alterations in metabolic profiles of the human brain

To investigate whether changes in metabolic profiles occur with aging, we characterized the metabolites in these human brain samples (i.e., the CVS/FA ratio) after splitting the participants into two age groups (Figure 6A): individuals in their 20s (18–29 years old, referred to as "20s") and those aged 40–60 years old (referred to as "≥40"). There were 208 compounds identified as showing significant age-related uptake or release differences (Figure 6B). We categorized these compounds into 10 patterns (Figures 6C–6E).

The top three patterns identified were as follows: (1) 53 compounds were taken up by the brain in the 20s age group but tended to remain stable in the ≥40 age group; (2) 51 compounds

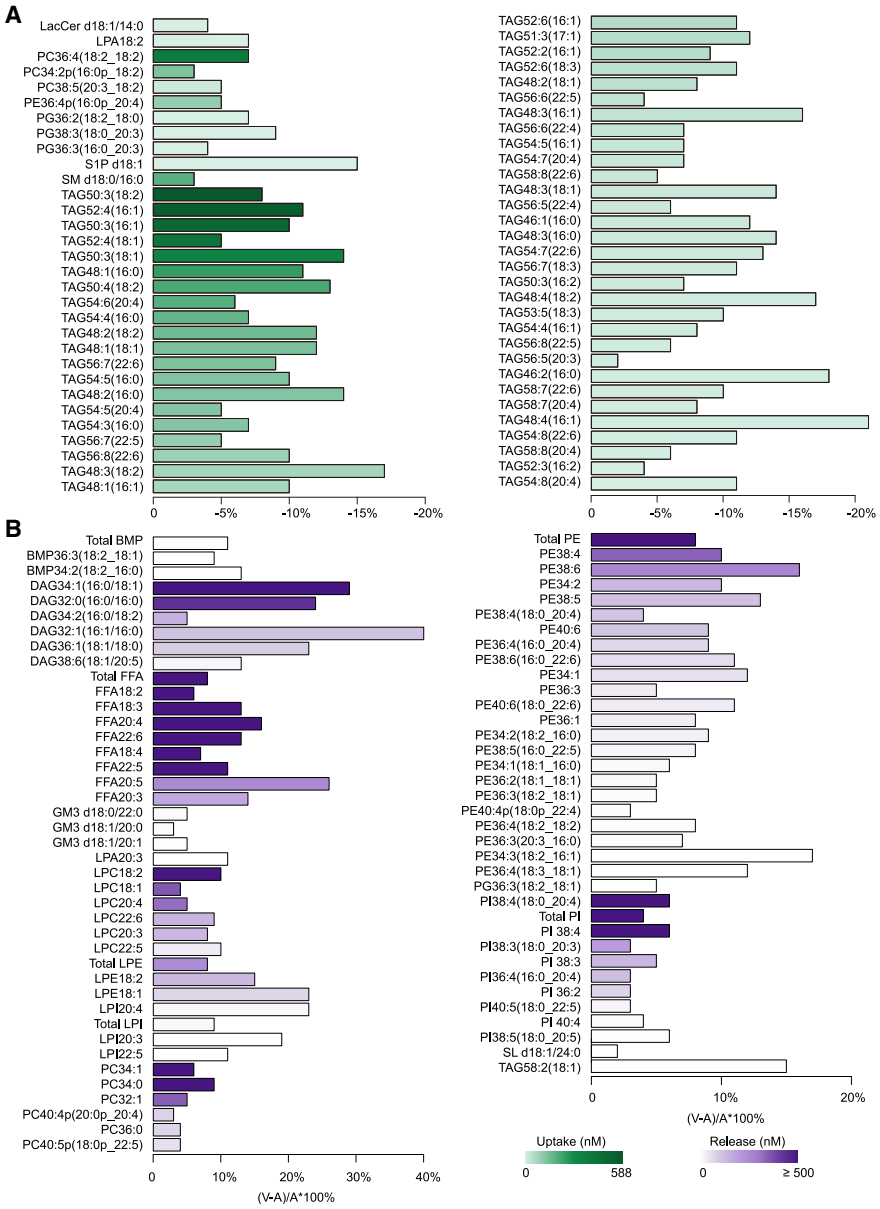

Figure 5. Lipid uptake and release by the human brain

The net uptake (A) and release (B) in nanomoles per liter of blood flowing through the brain and the ratios of lipids consumed by the human brain. Bar colors denote lipid uptake or release, whereas the intensity of the shading reflects the absolute quantities of net uptake or release. The lengths of the bars represent the uptake (A) or release (B) ratios of the corresponding lipids.

were taken up by and released from the brain in a balanced manner during the 20s age group, but they were predominantly released by the brain after the age of 40; and (3) 54 compounds were released by the brain in the 20s age group but became stable metabolites in the ≥40 age group. Notably, no compound was found to be taken up more by the human brain in the ≥40 age group relative to its uptake in the 20s age group (Figure 6D).

8-hydroxyquinoline is not a naturally occurring metabolite and has been used in drug development for the treatment of neurodegenerative disorders.[34] It showed a net uptake of 7.9% in the brains of individuals in their 20s, whereas the relative percentages remained stable (median of 5.1%) in those over 40. Similarly, indole-3-acrylic acid, a tryptophan catabolite, showed a net uptake of 7.9% for individuals in their 20s but remained stable (median ratio of 1.4%) for those over 40. Moreover, uridine, a pyrimidine nucleoside, exhibited substantial uptake by the brain at a ratio of 20.5% in the younger population as compared with a net balance among individuals over 40 years old. By contrast, phosphocholine and 1-methyladenosine tended to be released from the brain in the older population (with median ratios of 9.5% and 7.9%, respectively) but remained stable in the younger population.

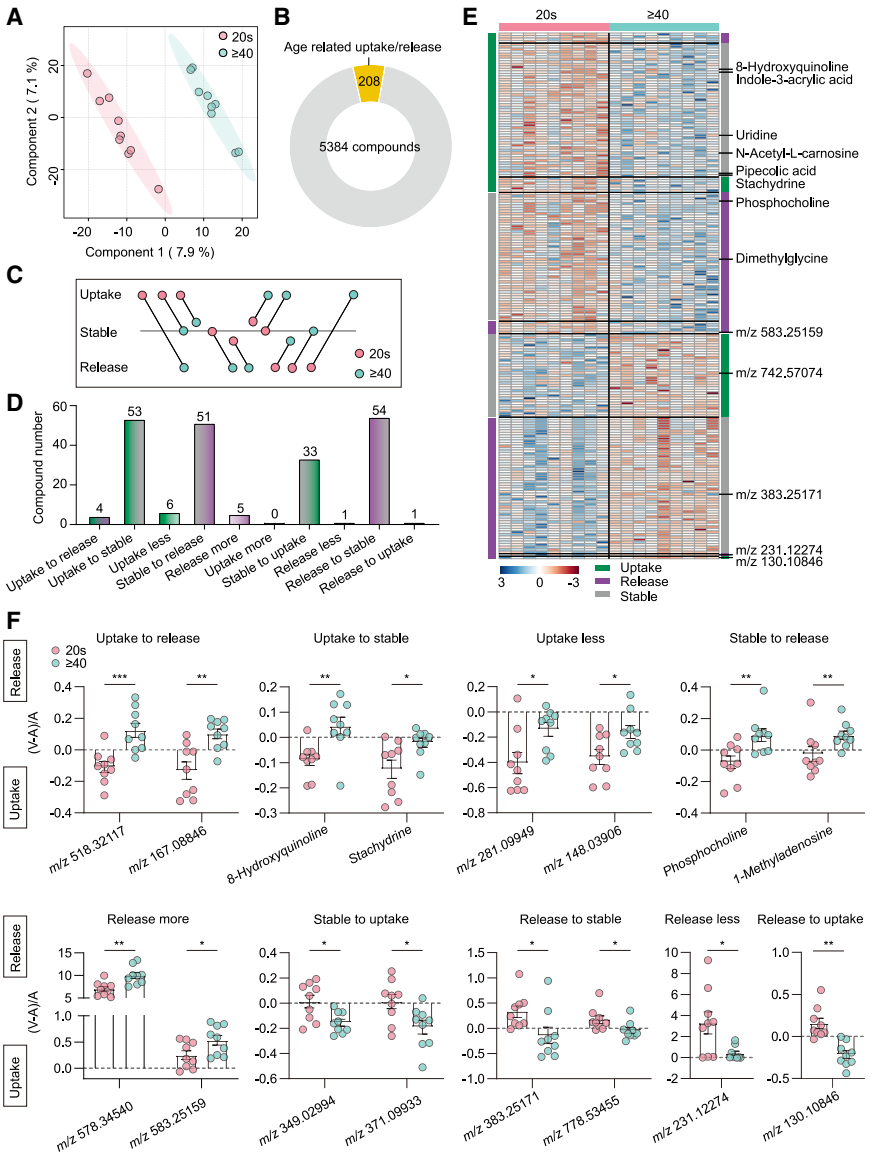

Figure 6. Age-related effects on brain metabolite uptake and release

(A) A partial least-squares discriminant analysis (PLS-DA) of CVS/FA (i.e., V/A) ratios for all detected compounds in the 28 participants divided into two age groups: individuals aged 18–29 years (n = 9, i.e., the 20s group) and those 40–60 years (n = 9, i.e., the ≥ 40 group).

(B) Donut chart showing the compounds with significant differences in age-related uptake or release. Significance between the two groups was determined by two-tailed paired t tests ($p < 0.05$).

(C) Schematic representation of the 10 patterns of age-related effects on metabolite uptake and release.

(D) Number of metabolites and ion features with age-related uptake or release patterns as shown in (C).

(E) Heatmap displaying (V − A)-to-A ratios of the 208 compounds with age-related uptake or release relative to (B–D) in the individuals in their 20s versus those ≥ 40. The scale bar indicates the relative (V−A)-to-A ratios in each sample.

(F) Scatter and bar graphs of representative metabolites and features with age-related uptake or release in the 20s group versus the over 40s group, following the patterns described in (C)–(E). Data presented as means with standard error bars; n = 9 for each group. Significance assessed by two-tailed t test. *$p < 0.05$, **$p < 0.01$, ***$p < 0.001$, ****$p < 0.0001$.

Additionally, we observed age-related changes in brain uptake/release for several unknown compounds. For instance, mass-to-charge ratio (m/z) 518.32117 had a net uptake of 10.5% in the brains of individuals in their 20s but a net release of 8.0% in those over 40. Upon further investigation, we determined the elemental composition of this metabolite to be C26H48NO7P, on the basis of which the neutral structure was speculated to be LysoPC (18:3(9Z,12Z,15Z)).

Through correlation analysis, we found that with age, the brain consumed less glucose, taurine, and 3MGA, while releasing more asparagine, biliverdin, choline, trimethylamine, and caprylate (Figures S7A–S7H). There were no age-related changes in lactate, glutamate, or glutamine (Figures S7I–S7K). Among lipids, the brain consumed more TAG, such as TAG48:3(18:1), TAG48:2(18:1), TAG48:3(16:0), TAG48:3(16:1), TAG50:4(18:2), TAG48:2(16:0), PG38:3(18:0_20:3), and PG36:2(18:2_18:0), but less SM d18:0/16:0 (Figures S8A–S8I). Additionally, there was a decrease in PE40:6 and an increase in LPE18:1, LPE18:2, LPC18:1, LPC20:3, and LPC20:4 with age (Figures S8J–S8O).

Comparison of substance exchange in the brain of patients with CVSS versus CVST

Cerebral venous sinus thrombosis (CVST) and non-thrombotic cerebral venous sinus stenosis (CVSS) exhibit similar symptoms, yet they represent distinct stroke subtypes.[35] We obtained distinct metabolomic profiles between CVSS and CVST patients (Figures 7A and 7B). The brains of CVSS patients absorbed 805 metabolites and 26 lipids while releasing 593 metabolites and 54 lipids. By contrast, CVST brains demonstrated reduced absorption and release of metabolites and lipids (Figure 7C).

The differential metabolites of the two groups were enriched in the pathways of carnitine synthesis, transfer of acetyl groups into mitochondria, tricarboxylic acid (TCA) cycle, glycolysis, etc. (Figure 7D). CVSS brains consumed more glucose and lactate, while releasing more byproducts of glucose metabolism, including pyruvate, succinate, and malate, indicating the increased glucose utilization but reduced mitochondrial utilization of glucose-derived substrates through oxidative phosphorylation in CVSS brains compared with CVST brains. CVST brains consumed more tryptophan,

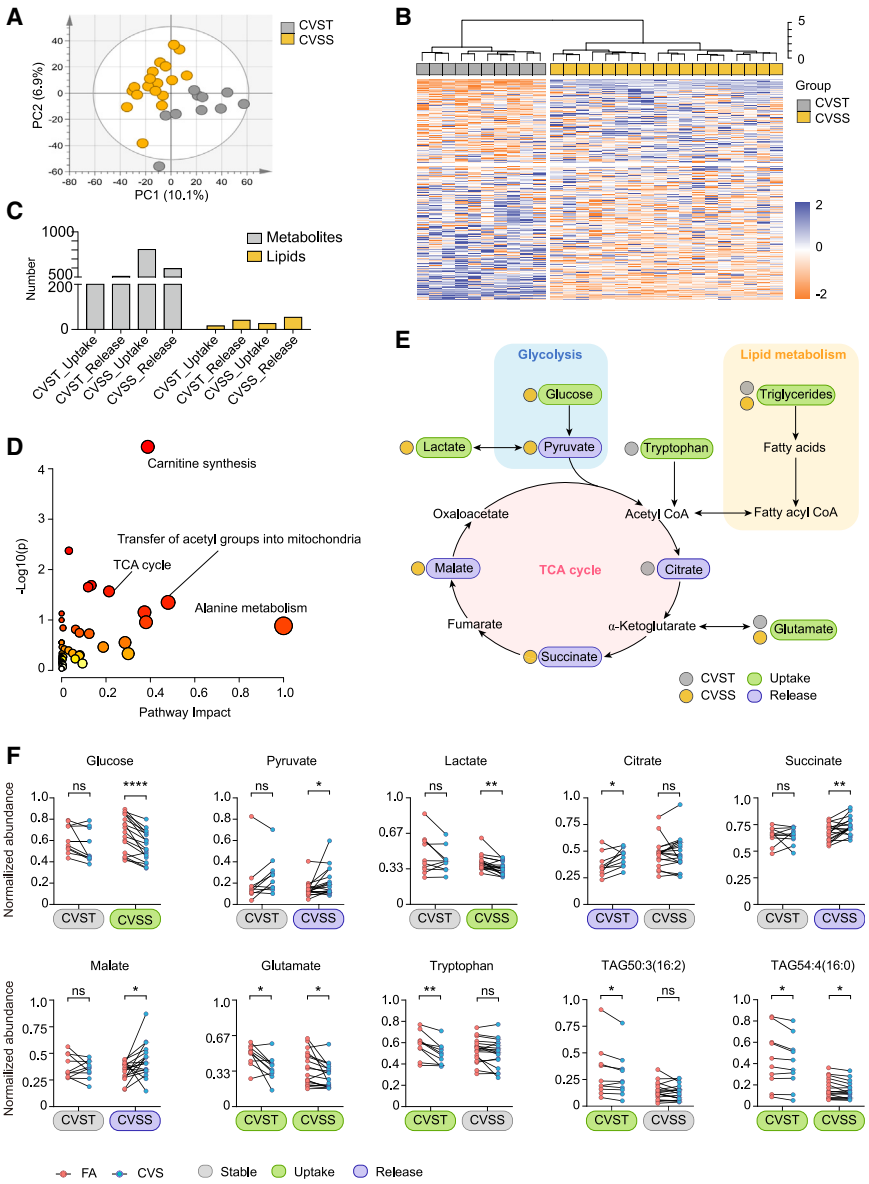

Figure 7. Comparison of metabolite and lipid exchange in the brain of patients with CVST versus CVSS

(A) PCA plot of CVS/FA ratios for all detected compounds in the patients with CVSS and CVST.

(B) Heatmap of CVS/FA ratios of differential metabolites in the patients. The scale bar indicates the relative CVS/FA ratios in each sample.

(C) Number of metabolites and lipids with uptake/release differences.

(D) Pathway analysis for metabolites exhibiting uptake/release differences in the patients.

(E) Summary diagram displaying metabolites and lipids in the pathways, including glycolysis, TCA cycle, and lipid metabolism with uptake/release differences.

(F) Scatter plots display relative abundance of metabolites and lipids in CVS and FA of CVST and CVSS groups. Significance was determined using *p* values after a two-tailed paired t test or one-sample Wilcoxon test. $*p < 0.05$, $**p < 0.01$, $****p < 0.0001$. CVST, $n = 10$; CVSS, $n = 18$ subjects.

TAG50:3(16:2) and TAG54:4(16:0), and released more citrate but consumed less glucose and lactate (Figures 7E and 7F; Table S2).

Metabolomic analysis of follow-up patients with cerebral venous stent implantation

We analyzed and compared the group of patients under general anesthesia with those who only received local anesthesia. The unsupervised analysis of metabolomic circulating levels in subjects under both anesthesia conditions showed clear overlap in the PCA plot, indicating minimal differences between them. In the clustering analysis, the samples from both anesthesia conditions were interspersed and closely located, suggesting minimal or no significant separation (Figure 8A and 8B).

Some of these patients were willing to return for follow-up visits. We examined various clinical parameters, including their symptoms and imaging indicators, and confirmed that these parameters showed no significant differences from healthy individuals (Table S1). We collected arterial and venous plasma samples under local anesthesia (retained spontaneous breathing and consciousness) from 8 subjects who had been followed up for more than a year after stent implantation. We observed that the brain arterial and venous metabolomic data from these individuals were similar to the data from the initial 28 subjects (Figures 8C–8E). For example, this dataset confirmed significant brain uptake of glucose, carnitine, methionine, tyrosine, and 3-indoxyl sulfate, as well as significant brain release of asparagine, glutamine, and pyroglutamic acid. Additionally, two previously uncertain ion features (*m/z* 115.03862 and *m/z* 203.05178) were again validated in this dataset as being absorbed by the brain (Figure 8F). Taken together, despite these potential confounding factors, our study strives to provide comprehensive data on metabolic uptake and release by the human brain under physiological conditions.

DISCUSSION

Understanding the brain's metabolic dynamics offers valuable insights into the intricate relationship between metabolism and higher cognitive functions. The earliest studies on substrate utilization in the brain, conducted from the late 1920s to the 1930s, revealed that carbohydrates are the primary fuel for the brain. Himwich and Nahum measured arteriovenous differences across the brains of dogs.[36] In 1942, Gibbs et al. confirmed these differences

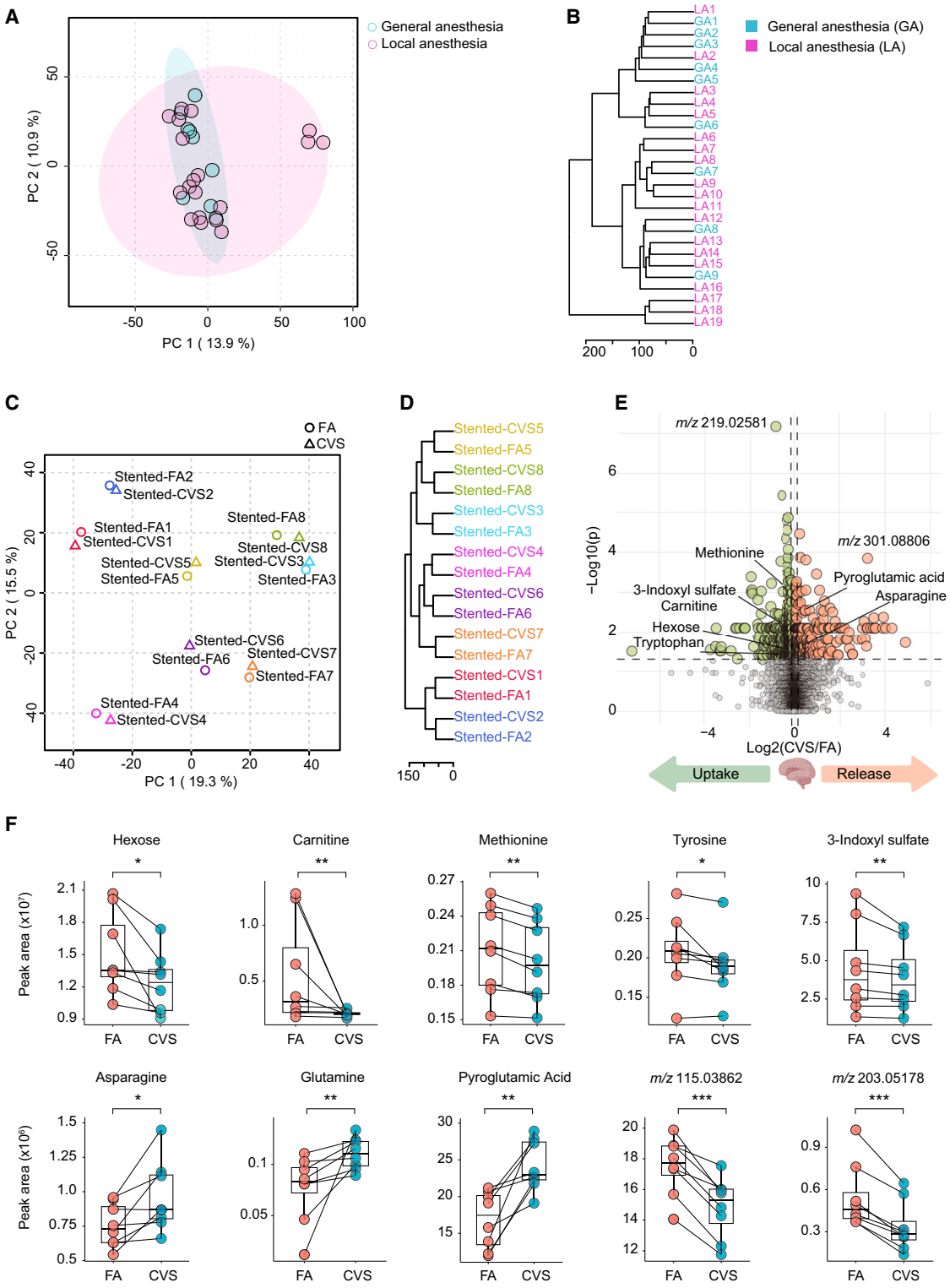

Figure 8. Metabolite profiling of brain arteriovenous samples from 8 subjects with cerebral venous stent implantation

(A and B) Comparison of plasma metabolome profiles of participants under general (n = 9) or local anesthesia (n = 19). PCA plot showing relative peak areas for all detected compounds in patients under general or local anesthesia (A). Hierarchical clustering dendrogram of relative peak areas for all detected compounds in the femoral arteries of participants (B).

(C) PCA of untargeted metabolomic data from samples of the 8 follow-up subjects.

(legend continued on next page)

(O_2, CO_2, pH value, lactate, sugar, total base, and inorganic phosphorus) in the human brain.[17] We detected over a thousand metabolites that demonstrated significant brain- or leg-specific exchange across the circulation. ^{18}F-fluoro-2-deoxyglucose (FDG), a glucose analog, is widely used in functional studies and clinical diagnostics for positron emission tomography (PET) imaging to assess glucose uptake capacity and localized metabolic activity in the brain.[37–41] The metabolites identified in our study as being taken up by the brain could serve as potential PET biomarkers for various neurological diseases in the future.

The absolute net uptake and release of metabolites per minute for an adult human brain could be further inferred (Table S2), assuming cerebral blood flow (CBF) of 0.55 ml/g brain tissue/min and brain weight of 1,407 g given in previous literatures.[42,43] Among the well-known classical metabolites quantified for net metabolic activity across the brain, glucose and glutamate were prominent. Glucose underwent a net uptake by the human brain of 15.9% (~91.52 mg/min). Regarding the net release or lack of absorption of hexose in a few individuals, this fluctuation is due to a combination of net exchange and inherent measurement bias of the instrument. Quality control (QC) samples themselves had a relative standard deviation of 5.7% throughout the entire measurement batch. Glutamate showed a net uptake in our study, contrary to some previous findings.[19] Lactate, an essential energy source for brain cells,[1] demonstrated a net uptake of 8.8%. Previous studies have shown conflicting results on lactate exchange,[29] which showed the brain absorbs lactate,[44] or releases it,[45–47] or show no exchange.[48] In our study, venous samples were collected from the confluence of sinuses, transverse sinus, sigmoid sinus, or the jugular bulb—sites that directly drain the brain, thereby excluding contributions from non-brain head tissues. The methodological distinction may account for discrepancies observed among different studies.

Pyruvate, another significant energy source for neurons,[1] had a net release of 32.98%, consistent with previous findings.[18] Oleamide, discovered in human serum,[49] affects various receptors involved in sleep regulation and memory.[50] Hypoxanthine is believed to enter the brain and be converted into purine nucleotides,[21] but its uptake ratio and absolute amount have not been determined previously. VC, which occurs naturally in citrus fruits and vegetables, is an essential nutrient and a recognized antioxidant molecule in the brain, with potential therapeutic roles against neurodegenerative diseases.[51] Our data indicated a slight net uptake of VC by the human brain. The results from arteriovenous lipidomics suggest that TAG serves as a valuable energy source for the brain. Their functional mechanisms and metabolic fates in the brain remain to be determined. One limitation of this study is the reliance on literature-based plasma concentrations of some metabolites, CBF, and brain mass estimates for calculations. Variations in individual physiological parameters and measurement conditions may result in inaccuracies.

The age-related correlation suggested that the consumption of glucose, taurine, and 3MGA by the brain decreases with age (Figures S7A–S7C), which is reasonable considering that the metabolic activity of the aging brain tends to decline. As age progresses, the brain releases increasing amounts of several small-molecule metabolites (e.g., asparagine, biliverdin, and choline) (Figures S7D–S7H) and lipids (e.g., LPE18:1, LPE18:2, and Land PC18:1) (Figure S8). There was no correlation between age and either brain blood flow or white matter volume (Figures S9A–S9C). Correlation analysis showed that with age, the volume of gray matter reduced, as did the brain's uptake of 3MGA (Figure S9D). Other metabolites with brain absorption and release that changed with age (i.e., glucose and taurine) showed no correlation with gray matter volume (Figures S9E–S9K). We further detected that the correlation between age and the absorption/release of metabolites and lipids in the legs did not resemble the findings observed in the brain (Figure S10).

CVSS is a significant factor in the pathogenesis of idiopathic intracranial hypertension, with high intracranial pressure, headache, transient visual obscuration, pulsatile tinnitus, etc.[35] CVST is an important subtype of stroke in young adults with thrombus in the cerebral dural veins or sinuses, caused by imbalances in pro-thrombotic and thrombolytic processes.[35] There are many overlapping symptoms between CVST and CVSS. We observed the CVST patients had reduced glucose requirements of the brain and reduced metabolic production of aerobic breakdown of glucose. This result may be explained by the CVST's reduced cerebral supply of blood and oxygen, hypercoagulable state of blood, and deteriorated microcirculation in the brain.[35,52]

To demonstrate that clinical diagnosis and age do not have an interaction effect, allowing for the combined analysis of metabolomics data as a single cohort, we performed a two-way ANOVA, including disease subtype and age as factors, as well as their interaction term. The results showed that the interaction terms of the plasma metabolome in these participants were not significant (false discovery rate [FDR] > 0.05) (Table S2), indicating that disease subtype and age have independent effects with no interaction. This suggests that the data can be combined for analysis. Additionally, we built linear regression models for the plasma metabolome in these participants that included disease subtype, age, and their interaction term. In these models, the interaction terms were not significant (FDR > 0.05) (Table S2), further supporting the conclusion that the effects of disease subtype and age on the metabolomics data are independent.

The arteriovenous data presented in this study were obtained from human subjects under anesthesia after overnight fasting, aiming to approximate a resting state as closely as possible. Given this fasted state, there is the possibility of increased lipid utilization and decreased carbohydrate utilization. However, it is important to acknowledge that the effects of anesthesia and fasting on brain metabolic exchange activity can be

(D) Hierarchical clustering dendrogram of plasma samples from FA and CVS of the 8 subjects.
(E) Volcano plots illustrating metabolites taken up and released by the brains of the 8 subjects. Unknown metabolites are indicated by their m/z values. Significance was determined using two-tailed paired t tests or one-sample Wilcoxon tests. The horizontal dashed line represents $p = 0.05$.
(F) Representative metabolites and features taken up and released by the brains of the 8 subjects. Box plots depict the median and lower and upper quartiles. Significance was determined using p values from a two-tailed paired t test or one-sample Wilcoxon test. $^{*}p < 0.05$, $^{**}p < 0.01$, $^{***}p < 0.001$.

unpredictable, and caution should be exercised when drawing conclusions about all metabolites.

RESOURCE AVAILABILITY

Lead contact

Further information and requests should be directed to Woo-ping Ge (woopingge@cibr.ac.cn).

Materials availability

This study did not generate new, unique reagents.

Data and code availability

The data generated and/or analyzed in this study are available from the corresponding authors upon reasonable request.

ACKNOWLEDGMENTS

We thank the members of the Ge laboratory for their advice and Xiaoqing Li, Yupeng Zhang, and Lingling Jiang for their assistance during blood collection. This work received support from the CAMS Innovation Fund for Medical Sciences (CIFMS, 2024-I2M-ZD-012), STI2030-Major Projects 2022ZD0204700, the National Natural Science Foundation of China (no. 32170964), the Youth Beijing Scholar Program (no. 065), and funds from the CIBR and Changping Laboratory to W.-P.G. This work also received support from the Beijing Municipal Science and Technology Commission (no. Z221100007422053) to D.M., the National Natural Science Foundation of China (no. 81825007), the Capital's Funds for Health Improvement and Research (no. 2022-2-2045), the National Key R&D Program of China (2022YFF1501500-5, 2017YFC1307900, and 2017YFC1307905), the Youth Beijing Scholar Program (no. 010), the Beijing Laboratory of Oral Health (no. PXM2021_014226_000041), the Beijing Talent Project (no. 2018A12), the Beijing Outstanding Young Scientist Program (no. BJJWZYJH01201910025030), and the National Ten-Thousand Talent Plan to Y.W.

AUTHOR CONTRIBUTIONS

W.-P.G. conceived the project. W.-P.G. and Y.W. supervised the project. L.Z., W.-P.G., Y.W., and D.M. designed the experiments. D.M., N.W., and B.Q. collected human blood samples. N.W. separated plasma from blood. L.Z. extracted metabolites. L.Z., X.Y., X.S., and Z.L. performed HPLC-MS and ion chromatography. L.Z. performed untargeted and in-house matched metabolomics analyses. X.Y., D.Y., Z.L., J.Y., M.H., and T.L. established the in-house metabolite library, and L.Z. and Y.X. completed standard curve generation and absolute quantification of metabolites. Z.B. drew the schematic diagram of the patient's blood collection. L.Z. prepared all figures. W.-P.G., Y.W., and X.J. provided reagents. L.Z. and W.-P.G. wrote the manuscript. All authors discussed, reviewed, and edited the manuscript.

DECLARATION OF INTERESTS

The authors declare no competing interests.

STAR★METHODS

Detailed methods are provided in the online version of this paper and include the following:

- KEY RESOURCES TABLE
- METHOD DETAILS
  - Participant enrollment
  - Blood sample collection procedure
  - Metabolite extraction
  - Metabolomic analysis by LC-MS/MS
  - QC and compound identification
  - HPLC-MS data processing and compound identification
  - Measurement of sugars and metabolites of the tricarboxylic acid (TCA) cycle
  - Lipid extraction
  - Lipidome measurement and quantification
  - Arteriography image acquisition, preprocessing, and time density curve (TDC) parameter calculation
  - Magnetic resonance imaging data acquisition and brain volume analysis
  - Stable isotope tracing of metabolites in mice
  - Statistical analysis and data visualization

SUPPLEMENTAL INFORMATION

Supplemental information can be found online at https://doi.org/10.1016/j.neuron.2025.03.003.

Received: May 25, 2024
Revised: December 6, 2024
Accepted: March 3, 2025
Published: March 26, 2025

REFERENCES

1. Bélanger, M., Allaman, I., and Magistretti, P.J. (2011). Brain energy metabolism: focus on astrocyte-neuron metabolic cooperation. Cell Metab. *14*, 724–738. https://doi.org/10.1016/j.cmet.2011.08.016.
2. Magistretti, P.J., and Allaman, I. (2015). A cellular perspective on brain energy metabolism and functional imaging. Neuron *86*, 883–901. https://doi.org/10.1016/j.neuron.2015.03.035.
3. Mink, J.W., Blumenschine, R.J., and Adams, D.B. (1981). Ratio of central nervous system to body metabolism in vertebrates: its constancy and functional basis. Am. J. Physiol. *241*, R203–R212. https://doi.org/10.1152/ajpregu.1981.241.3.R203.
4. Ding, J., Ji, J., Rabow, Z., Shen, T., Folz, J., Brydges, C.R., Fan, S., Lu, X., Mehta, S., Showalter, M.R., et al. (2021). A metabolome atlas of the aging mouse brain. Nat. Commun. *12*, 6021. https://doi.org/10.1038/s41467-021-26310-y.
5. Wyss-Coray, T. (2016). Ageing, neurodegeneration and brain rejuvenation. Nature *539*, 180–186. https://doi.org/10.1038/nature20411.
6. Rasmussen, M.K., Mestre, H., and Nedergaard, M. (2022). Fluid transport in the brain. Physiol. Rev. *102*, 1025–1151. https://doi.org/10.1152/physrev.00031.2020.
7. Louveau, A., Plog, B.A., Antila, S., Alitalo, K., Nedergaard, M., and Kipnis, J. (2017). Understanding the functions and relationships of the glymphatic system and meningeal lymphatics. J. Clin. Invest. *127*, 3210–3219. https://doi.org/10.1172/jci90603.
8. Zlokovic, B.V. (2008). The blood-brain barrier in health and chronic neurodegenerative disorders. Neuron *57*, 178–201. https://doi.org/10.1016/j.neuron.2008.01.003.
9. Murashige, D., Jang, C., Neinast, M., Edwards, J.J., Cowan, A., Hyman, M.C., Rabinowitz, J.D., Frankel, D.S., and Arany, Z. (2020). Comprehensive quantification of fuel use by the failing and nonfailing human heart. Science *370*, 364–368. https://doi.org/10.1126/science.abc8861.
10. Jang, C., Hui, S., Zeng, X., Cowan, A.J., Wang, L., Chen, L., Morscher, R.J., Reyes, J., Frezza, C., Hwang, H.Y., et al. (2019). Metabolite Exchange between Mammalian Organs Quantified in Pigs. Cell Metab. *30*, 594–606.e3. https://doi.org/10.1016/j.cmet.2019.06.002.
11. Xiong, N., Gao, X., Zhao, H., Cai, F., Zhang, F.C., Yuan, Y., Liu, W., He, F., Zacharias, L.G., Lin, H., et al. (2020). Using arterial-venous analysis to characterize cancer metabolic consumption in patients. Nat. Commun. *11*, 3169. https://doi.org/10.1038/s41467-020-16810-8.
12. Blazey, T., Snyder, A.Z., Goyal, M.S., Vlassenko, A.G., and Raichle, M.E. (2018). A systematic meta-analysis of oxygen-to-glucose and

oxygen-to-carbohydrate ratios in the resting human brain. PLoS One *13*, e0204242. https://doi.org/10.1371/journal.pone.0204242.

13. Boyle, P.J., Scott, J.C., Krentz, A.J., Nagy, R.J., Comstock, E., and Hoffman, C. (1994). Diminished brain glucose metabolism is a significant determinant for falling rates of systemic glucose utilization during sleep in normal humans. J. Clin. Invest. *93*, 529–535. https://doi.org/10.1172/jci117003.
14. Mergenthaler, P., Lindauer, U., Dienel, G.A., and Meisel, A. (2013). Sugar for the brain: the role of glucose in physiological and pathological brain function. Trends Neurosci. *36*, 587–597. https://doi.org/10.1016/j.tins.2013.07.001.
15. Himwich, H.E., and Fazekas, J.F. (1937). The effect of hypoglycemia on the metabolism of the brain. Endocrinology *21*, 800–807. https://doi.org/10.1210/endo-21-6-800.
16. Scheinberg, P., and Stead, E.A. (1949). The cerebral blood flow in male subjects as measured by the nitrous oxide technique. normal values for blood flow, oxygen utilization, glucose utilization, and peripheral resistance, with observations on the effect of tilting and anxiety. J. Clin. Invest. *28*, 1163–1171. https://doi.org/10.1172/jci102150.
17. Gibbs, E.L., Lennox, W.G., Nims, L.F., and Gibbs, F.A. (1942). Arterial and cerebral venous blood: arterial-venous differences in man. J. Biol. Chem. *144*, 325–332. https://doi.org/10.1016/S0021-9258(18)72512-X.
18. Himwich, W.A., and Himwich, H.E. (1946). Pyruvic acid exchange of the brain. J. Neurophysiol. *9*, 133–136. https://doi.org/10.1152/jn.1946.9.2.133.
19. Berg, A., Bellander, B.M., Wanecek, M., Norberg, A., Ungerstedt, U., Rooyackers, O., and Wernerman, J. (2008). The pattern of amino acid exchange across the brain is unaffected by intravenous glutamine supplementation in head trauma patients. Clin. Nutr. *27*, 816–821. https://doi.org/10.1016/j.clnu.2008.06.006.
20. Wishart, D.S. (2019). Metabolomics for Investigating Physiological and Pathophysiological Processes. Physiol. Rev. *99*, 1819–1875. https://doi.org/10.1152/physrev.00035.2018.
21. Spector, R. (1988). Hypoxanthine transport and metabolism in the central nervous system. J. Neurochem. *50*, 969–978. https://doi.org/10.1111/j.1471-4159.1988.tb03006.x.
22. Ipata, P.L., Camici, M., Micheli, V., and Tozz, M.G. (2011). Metabolic network of nucleosides in the brain. Curr. Top. Med. Chem. *11*, 909–922. https://doi.org/10.2174/156802611795347555.
23. Gessner, P., Lum, J., and Frenguelli, B.G. (2023). The mammalian purine salvage pathway as an exploitable route for cerebral bioenergetic support after brain injury. Neuropharmacology *224*, 109370. https://doi.org/10.1016/j.neuropharm.2022.109370.
24. Frenguelli, B.G. (2019). The Purine Salvage Pathway and the Restoration of Cerebral ATP: Implications for Brain Slice Physiology and Brain Injury. Neurochem. Res. *44*, 661–675. https://doi.org/10.1007/s11064-017-2386-6.
25. Lying-Tunell, U., Lindblad, B.S., Malmlund, H.O., and Persson, B. (1980). Cerebral blood flow and metabolic rate of oxygen, glucose, lactate, pyruvate, ketone bodies and amino acids. Acta Neurol. Scand. *62*, 265–275. https://doi.org/10.1111/j.1600-0404.1980.tb03035.x.
26. Grill, V., Björkman, O., Gutniak, M., and Lindqvist, M. (1992). Brain uptake and release of amino acids in nondiabetic and insulin-dependent diabetic subjects: important role of glutamine release for nitrogen balance. Metabolism *41*, 28–32. https://doi.org/10.1016/0026-0495(92)90186-e.
27. Fernstrom, J.D., and Fernstrom, M.H. (2007). Tyrosine, phenylalanine, and catecholamine synthesis and function in the brain. 1548S. J. Nutr. *137*, 1539S. https://doi.org/10.1093/jn/137.6.1539S.
28. Swann, J.R., Spitzer, S.O., and Diaz Heijtz, R. (2020). Developmental Signatures of Microbiota-Derived Metabolites in the Mouse Brain. Metabolites *10*, 172. https://doi.org/10.3390/metabo10050172.
29. Magistretti, P.J., and Allaman, I. (2018). Lactate in the brain: from metabolic end-product to signalling molecule. Nat. Rev. Neurosci. *19*, 235–249. https://doi.org/10.1038/nrn.2018.19.
30. Chu, C., Murdock, M.H., Jing, D., Won, T.H., Chung, H., Kressel, A.M., Tsaava, T., Addorisio, M.E., Putzel, G.G., Zhou, L., et al. (2019). The microbiota regulate neuronal function and fear extinction learning. Nature *574*, 543–548. https://doi.org/10.1038/s41586-019-1644-y.
31. Rhea, E.M., and Banks, W.A. (2021). Interactions of Lipids, Lipoproteins, and Apolipoproteins with the Blood-Brain Barrier. Pharm. Res. *38*, 1469–1475. https://doi.org/10.1007/s11095-021-03098-6.
32. Banks, W.A., Farr, S.A., Salameh, T.S., Niehoff, M.L., Rhea, E.M., Morley, J.E., Hanson, A.J., Hansen, K.M., and Craft, S. (2018). Triglycerides cross the blood-brain barrier and induce central leptin and insulin receptor resistance. Int. J. Obes. (Lond) *42*, 391–397. https://doi.org/10.1038/ijo.2017.231.
33. Molenaar, M.R., Jeucken, A., Wassenaar, T.A., van de Lest, C.H.A., Brouwers, J.F., and Helms, J.B. (2019). LION/web: a web-based ontology enrichment tool for lipidomic data analysis. GigaScience *8*, giz061. https://doi.org/10.1093/gigascience/giz061.
34. Gupta, R., Luxami, V., and Paul, K. (2021). Insights of 8-hydroxyquinolines: A novel target in medicinal chemistry. Bioorg. Chem. *108*, 104633. https://doi.org/10.1016/j.bioorg.2021.104633.
35. Meng, R., Dornbos, D., 3rd, Meng, L., Wu, Y., Liu, Y., Li, G., Li, G., Li, S., Sun, F., Wang, X., et al. (2012). Clinical differences between acute CVST and non-thrombotic CVSS. Clin. Neurol. Neurosurg. *114*, 1257–1262. https://doi.org/10.1016/j.clineuro.2012.03.036.
36. Himwich, H.E., and Nahum, L.H. (1929). Respiratory Quotient of the Brain. Proc. Soc. Exp. Biol. Med. *26*, 496–497. https://doi.org/10.3181/00379727-26-4362.
37. Aide, N., Hicks, R.J., Le Tourneau, C., Lheureux, S., Fanti, S., and Lopci, E. (2019). FDG PET/CT for assessing tumour response to immunotherapy : Report on the EANM symposium on immune modulation and recent review of the literature. Eur. J. Nucl. Med. Mol. Imaging *46*, 238–250. https://doi.org/10.1007/s00259-018-4171-4.
38. Uslu, L., Donig, J., Link, M., Rosenberg, J., Quon, A., and Daldrup-Link, H.E. (2015). Value of 18F-FDG PET and PET/CT for evaluation of pediatric malignancies. J. Nucl. Med. *56*, 274–286. https://doi.org/10.2967/jnumed.114.146290.
39. Wong, W.L. (2021). PET-CT for Staging and Detection of Recurrence of Head and Neck Cancer. Semin. Nucl. Med. *51*, 13–25. https://doi.org/10.1053/j.semnuclmed.2020.09.004.
40. Kawai, N., Miyake, K., Yamamoto, Y., Nishiyama, Y., and Tamiya, T. (2013). 18F-FDG PET in the diagnosis and treatment of primary central nervous system lymphoma. BioMed Res. Int. *2013*, 247152. https://doi.org/10.1155/2013/247152.
41. Shivamurthy, V.K.N., Tahari, A.K., Marcus, C., and Subramaniam, R.M. (2015). Brain FDG PET and the diagnosis of dementia. AJR Am. J. Roentgenol. *204*, W76–W85. https://doi.org/10.2214/ajr.13.12363.
42. Slupe, A.M., and Kirsch, J.R. (2018). Effects of anesthesia on cerebral blood flow, metabolism, and neuroprotection. J. Cereb. Blood Flow Metab. *38*, 2192–2208. https://doi.org/10.1177/0271678x18789273.
43. Molina, D.K., and DiMaio, V.J.M. (2012). Normal organ weights in men: part II-the brain, lungs, liver, spleen, and kidneys. Am. J. Forensic Med. Pathol. *33*, 368–372. https://doi.org/10.1097/PAF.0b013e31823d29ad.
44. Mcginty, D.A. (1929). The regulation of respiration: XXV. Variations in the lactic acid metabolism in the intact brain. Am. J. Physiol. *88*, 312–325. https://doi.org/10.1152/ajplegacy.1929.88.2.312.
45. van Hall, G., Strømstad, M., Rasmussen, P., Jans, O., Zaar, M., Gam, C., Quistorff, B., Secher, N.H., and Nielsen, H.B. (2009). Blood lactate is an important energy source for the human brain. J. Cereb. Blood Flow Metab. *29*, 1121–1129. https://doi.org/10.1038/jcbfm.2009.35.

46. Quistorff, B., Secher, N.H., and Van Lieshout, J.J. (2008). Lactate fuels the human brain during exercise. FASEB J. *22*, 3443–3449. https://doi.org/10.1096/fj.08-106104.

47. Overgaard, M., Rasmussen, P., Bohm, A.M., Seifert, T., Brassard, P., Zaar, M., Homann, P., Evans, K.A., Nielsen, H.B., and Secher, N.H. (2012). Hypoxia and exercise provoke both lactate release and lactate oxidation by the human brain. FASEB J. *26*, 3012–3020. https://doi.org/10.1096/fj.11-191999.

48. Pere, P., Höckerstedt, K., Isoniemi, H., and Lindgren, L. (2000). Cerebral blood flow and oxygenation in liver transplantation for acute or chronic hepatic disease without venovenous bypass. Liver Transpl. *6*, 471–479. https://doi.org/10.1053/jlts.2000.8186.

49. Arafat, E.S., Trimble, J.W., Andersen, R.N., Dass, C., and Desiderio, D.M. (1989). Identification of fatty acid amides in human plasma. Life Sci. *45*, 1679–1687. https://doi.org/10.1016/0024-3205(89)90278-6.

50. Murillo-Rodríguez, E., Giordano, M., Cabeza, R., Henriksen, S.J., Méndez Díaz, M., Navarro, L., and Prospéro-García, O. (2001). Oleamide modulates memory in rats. Neurosci. Lett. *313*, 61–64. https://doi.org/10.1016/s0304-3940(01)02256-x.

51. Harrison, F.E., and May, J.M. (2009). Vitamin C function in the brain: vital role of the ascorbate transporter SVCT2. Free Radic. Biol. Med. *46*, 719–730. https://doi.org/10.1016/j.freeradbiomed.2008.12.018.

52. Nakase, H., Heimann, A., and Kempski, O. (1996). Alterations of regional cerebral blood flow and oxygen saturation in a rat sinus-vein thrombosis model. Stroke *27*, 720–728. https://doi.org/10.1161/01.str.27.4.720.

53. Forsberg, E.M., Huan, T., Rinehart, D., Benton, H.P., Warth, B., Hilmers, B., and Siuzdak, G. (2018). Data processing, multi-omic pathway mapping, and metabolite activity analysis using XCMS Online. Nat. Protoc. *13*, 633–651. https://doi.org/10.1038/nprot.2017.151.

54. Song, J.W., Lam, S.M., Fan, X., Cao, W.J., Wang, S.Y., Tian, H., Chua, G.H., Zhang, C., Meng, F.P., Xu, Z., et al. (2020). Omics-Driven Systems Interrogation of Metabolic Dysregulation in COVID-19 Pathogenesis. Cell Metab. *32*, 188–202.e5. https://doi.org/10.1016/j.cmet.2020.06.016.

55. Blaise, B.J., Correia, G.D.S., Haggart, G.A., Surowiec, I., Sands, C., Lewis, M.R., Pearce, J.T.M., Trygg, J., Nicholson, J.K., Holmes, E., and Ebbels, T.M.D. (2021). Statistical analysis in metabolic phenotyping. Nat. Protoc. *16*, 4299–4326. https://doi.org/10.1038/s41596-021-00579-1.

56. Dieterle, F., Ross, A., Schlotterbeck, G., and Senn, H. (2006). Probabilistic quotient normalization as robust method to account for dilution of complex biological mixtures. Application in 1H NMR metabonomics. Anal. Chem. *78*, 4281–4290. https://doi.org/10.1021/ac051632c.

STAR★METHODS

KEY RESOURCES TABLE

REAGENT or RESOURCE	SOURCE	IDENTIFIER
Chemicals		
Avertin	Sigma-Aldrich	Cat# T48402
Sodium Heparin	Solarbio	Cat# IH1440
Acetonitrile	Supelco	Cat# 100030
Water (LC-MS grade)	Supelco	Cat# 115333
Methanol (LC-MS grade)	Supelco	Cat# 106007
Isopropanol, Optima™LC/MS Grade	Thermo Fisher	Cat# A461-4
Formic acid, 99.0^{+}%, Optima™ LC/MS Grade	Thermo Fisher	Cat# A11750
Acetic acid, Optima™ LC/MS	Thermo Fisher	Cat# A11350
Ammonium formate	Merck	Cat# 70221
Ammonium acetate	Merck	Cat# 73594
Ammonium hydroxide solution	Sigma-Aldrich	Cat# 338818
Pierce™ LTQ Velos ESI Positive Ion Calibration Solution	Thermo Fisher	Cat# 88323
Pierce™ Negative Ion Calibration Solution	Thermo Fisher	Cat# 88324
0.9% NaCl	Beyotime Biotechnology	Cat# ST341
[U-13C]Glucose	MedChemExpress	Cat# HY-B0389A
[U-13C]Glutamate	MedChemExpress	Cat# HY-14608S5
Experimental models: Organisms/strains		
C57BL/6N	Charles River Laboratories	Strain code: 027; RRID:MGI:2159965
Software and algorithms		
GraphPad Prism v8 and v9	GraphPad	https://www.graphpad.com/; RRID:SCR_002798
MetaboAnalyst Version 5.0	MetaboAnalyst	https://www.metaboanalyst.ca/; RRID:SCR_015539
R Studio	R	https://www.rstudio.com/

METHOD DETAILS

Participant enrollment

We enrolled 28 participants who were undergoing interventional procedures for cerebral venous diseases. Prior to participation, all subjects or their legal guardians provided written informed consent after comprehensive discussions that included verbal and detailed explanations of the study. This study received approval from the ethical review board at Beijing Tiantan Hospital, Capital Medical University, under ethics review number KY 2020-112-03. There were five selection criteria for participants in this study. (1) Participants exhibited symptoms indicative of increased intracranial pressure. (2) Imaging examinations revealed evidence of venous sinus stenosis. (3) Individuals required venous sinus pressure measurement through an intracranial microcatheter. (4) Participants who had the potential need for transvenous lateral sinus stent placement were included. (5) The primary clinical diagnosis for these individuals was idiopathic intracranial hypertension with concurrent venous stenosis and/or chronic venous sinus thrombosis. Blood samples were collected during routine surgical procedures. The collection of blood samples was performed in a manner that did not interfere with or impact the participants' medical treatment.

Blood sample collection procedure

All participants adhered to an overnight fasting regimen before undergoing cerebral venous interventional surgery. During the surgical procedure, catheters were inserted into the femoral artery and femoral vein sheaths. Blood samples (1–2 ml) were drawn from both the femoral artery and femoral vein using sterile syringes. As the guide wire within the venous sheath reached specific anatomical locations, such as the jugular bulb, sigmoid sinus, transverse sinus, or confluence of sinuses, cerebral venous drainage blood was collected. This collection was facilitated by using a sterile syringe and a microcatheter.

After blood collection, the samples retained in the syringes were immediately transferred into vacutainers coated with lithium-heparin (BD, Cat# 367884) and were kept on ice. These samples were transported to the laboratory for further processing as described.[11] Notably, all collected blood samples underwent rigorous evaluation for hemolysis, and only those samples that exhibited no hemolysis were subjected to further analysis.

The samples were then centrifuged at 1,000*g* at 4°C for 10 min to separate the plasma from the cellular components. The plasma samples were then stored at –80°C until the metabolite extraction process was performed. It is important to emphasize that these stringent procedures were meticulously followed to ensure the quality and integrity of the collected blood samples, a critical factor in the subsequent metabolite analysis process.

Metabolite extraction

Plasma samples were removed from the –80°C freezer and placed on ice to thaw. A small amount of plasma (15 μl) was used for metabolite extraction. To precipitate proteins, 120 μl of a 90% (vol/vol) acetonitrile/water solution was added to the 15 μl of plasma. The mixture was vigorously vortexed for 5 min and then centrifuged at 21,130*g* for 15 min at 4°C (5424R, Eppendorf, Germany). Subsequently, 100 μl of the supernatant was collected for HPLC-MS analysis. The remaining supernatants from all samples were combined, vortexed, and subjected to a second centrifugation (21,130 *g*, 15 min, 4°C). The resulting pooled supernatant was divided into two equal portions. One half was used as a quality control (QC) sample for HPLC-MS analysis to assess instrument variability. The other half of the pooled supernatant was lyophilized in a centrifugal vacuum evaporator (JM-CV600, Beijing JM Technology, China) at 4°C. The freeze-dried pellet was subsequently reconstituted in 80% (vol/vol) acetonitrile/water, followed by vortexing and centrifugation (21,130*g*, 15 min, 4°C) to obtain an enriched pooled supernatant with a concentration three times that of the other samples. The enriched pooled samples were used for tandem mass spectrometry (MS/MS) analysis to increase the total number of identified metabolites.

Metabolomic analysis by LC-MS/MS

Metabolite measurements were conducted using high-resolution Quadrupole-Orbitrap mass spectrometers (Q Exactive, Thermo Fisher Scientific) operating in both negative and positive ion modes. These spectrometers were coupled with a HILIC-Z column (2.1 × 100 mm, 2.7 μm; InfinityLab Poroshell 120, Agilent) within a Vanquish UHPLC system (Thermo Fisher Scientific, USA).

For the positive ion mode, solvent A consisted of water with 10 mM ammonium formate and 0.14% (vol/vol) formic acid, whereas solvent B consisted of acetonitrile with 10 mM ammonium formate and 0.14% (vol/vol) formic acid. In the negative ion mode, solvent A comprised water with 10 mM ammonium acetate and 2 mM ammonium hydroxide, and solvent B was acetonitrile with 10 mM ammonium acetate and 2 mM ammonium hydroxide. Both modes used the same HILIC chromatographic separation with the following gradient parameters: 0–4 min from 100% to 84% B, 4–11 min from 84% to 40% B, 11–12 min maintained at 40% B, 12–13 min from 40% to 100% B, and 13–17 min re-equilibrated at 100% B. The autosampler was operated at 4°C, and the oven temperature was maintained at 35°C. The flow rate was 0.4 ml/min, and the injection volume was 3 μl. The ion source conditions were set as follows: spray voltage, 3.5 kV for the positive ion mode and 3.2 kV for the negative ion mode; sheath gas flow rate, 30 arbitrary units; auxiliary gas flow rate, 10 arbitrary units; sweep gas flow rate, 5 arbitrary units; capillary temperature, 320°C; S-lens RF level, 55; auxiliary gas heater temperature, 350°C.

Full MS data were acquired with the following parameters: resolution, 70,000; AGC target, 3e6; maximum IT, 100 ms; scan range, 60–900 *m/z*; spectrum data type, centroid. Data-dependent MS/MS (ddMS2) analysis was performed twice for a single enriched pooled sample, covering scan ranges of 60–400 and 350–900 *m/z*. The ddMS2 parameters were as follows: resolution, 17,500; AGC target, 5e4; maximum IT, 80 ms; loop count, 10; TopN, 10; isolation window, 1.6 *m/z*; dynamic first mass; NCE, 20, 30, and 40; spectrum data type, centroid; minimum AGC target, 1.0e3; intensity threshold, 1.3e4; exclude isotopes, on; dynamic exclusion, 6.0 s. Raw data were acquired using the Xcalibur software (Thermo Fisher Scientific).

QC and compound identification

To ensure the stability and reliability of our measurements, we analyzed all QC samples (i.e., an aliquot of pooled samples from the 28 participants) in each experimental batch. QC samples, derived from the plasma of study participants, were injected at the initiation of each batch and subsequently at intervals ranging from the 8th to the 12th injection within the batch. These QC samples were systematically analyzed within experimental batches to assess their consistency.

The cumulative peak areas of the QC samples across each batch exhibited remarkable reproducibility and stability, as evidenced by a relative standard deviation of 5.66% (Data not shown). This outcome underscores the favorable quality and reproducibility of our HPLC-MS data. Hierarchical clustering dendrogram analysis confirmed these results, with all QC samples forming cohesive clusters (Data not shown), indicating minimal variability and technical errors. Spearman-rank correlation analysis revealed robust correlations within the QC samples (rxy, 0.43–0.79) and comparatively lower correlations between the QC samples and the participants' samples (rxy, −0.42 to 0.33) (Table S2).

Among these absorbed or released compounds, 90 metabolites were identified based on accurate mass, fragment ion messages in MS/MS, and natural isotopic distribution, and 1,173 compounds were assigned predictive chemical formulas according to their accurate mass and natural isotopic distribution.

HPLC-MS data processing and compound identification

We conducted untargeted/global metabolomics investigations to ensure thorough coverage of the metabolome. First, the full MS dataset was converted into *.mzML files through ProteoWizard's MS Convert (Palo Alto, CA, USA). Subsequently, Scripps XCMSplus (La Jolla, CA, USA)[53] was used to extract and integrate ion features, unifying data from both electrospray ionization positive and negative modes. Full MS and ddMS2 data underwent processing using Compound Discoverer 3.2 software (Thermo Fisher Scientific). This involved three primary steps: (i) compound detection and peak alignment; (ii) querying major biomolecule and metabolomic databases such as mzCloud (https://www.mzcloud.org/), HMDB (https://hmdb.ca/), KEGG (https://www.kegg.jp/), MassBank (https://massbank.us/), Lipid MAPS (https://lipidmaps.org/), and Biocyc (https://www.biocyc.org/); and (iii) annotating and identifying untargeted data by aligning sample mass spectra with reference mass spectra. The identity verification of the detected compounds was carried out on two levels: MS1, involving an exact mass and retention time match to authenticated standards, and MS2, which focused on an examination of the fragment ion *m/z*.

In parallel, we assembled an in-house LC-MS library encapsulating 462 well-established small-molecule metabolites. This library furnished crucial information, including chromatographic retention time, exact mass, characteristic MS2 fragment ions and natural isotopic distributions. To enhance the precision of metabolite identification, we subsequently cross-referenced the raw data with our local library, considering factors such as accurate *m/z*, retention time, and fragment ion features. For the identification and quantification of metabolites, Tracefinder 5.1 software (Thermo Fisher Scientific) was used.

The compound in line 1537 of our raw data spreadsheet has the molecular formula C6H8O4 and a liquid chromatography retention time of 4.019 min. The non-targeted primary annotation (based on Compound Discoverer 3.2) is 2,3-Dimethylmaleate, but by cross-referencing with our in-house standard metabolite library, we further identified it as 3-methylglutaric acid (3MGA), with a molecular mass of 144.04092 and an m/z of 143.0339 in negative ion mode.

We also conducted an in-depth comparison of metabolite abundance between arterial and cerebral venous sinus (CVS) samples. Statistical significance was assessed using the false discovery rate (FDR)-adjusted two-tailed paired *t*-test or one-sample Wilcoxon test, contingent on the normality of the data distribution, with an FDR threshold of <0.05.

Measurement of sugars and metabolites of the tricarboxylic acid (TCA) cycle

We quantified the concentrations of sugars, specifically glucose and arabinose, as well as metabolites of the TCA cycle using high-performance ion chromatography (HPIC). In preparation for measurement, 20 μl of plasma was combined with 80 μl of cold extraction solvent (methanol/acetonitrile, 50:50, vol/vol), vigorously vortexed, and promptly centrifuged at 21,130*g* for 20 min at 4°C. The resulting supernatant was subjected to lyophilization in a centrifugal vacuum evaporator at 4°C. The freeze-dried pellet was then reconstituted in ultra-pure water, diluted to 10, 20, and 50 times the original plasma volume, and subsequently filtered through a 0.22-μm filter for subsequent analysis. For the HPIC analyses, 25 μl of the extracted sample solution was used. These analyses were conducted using an ICS6000 system (Thermo Fisher Scientific), which comprises two pumps, an amperometric detector, a conductivity detector, and an automated sampler equipped with a 25-μl injection loop. The Chromeleon Chromatography Management System (Thermo Fisher Scientific) was used for analyte identification and quantification.

The separation of monoses was carried out using an analytical CarboPac PA20 pellicular anion-exchange resin column (150 × 3 mm) with a preceding CarboPac PA20 guard column (30 mm× 3 mm). Elution of monoses was achieved using 30 mM NaOH at a flow rate of 0.4 ml/min. For the separation of organic acids, an AS11 analytical column (250 mm × 2 mm) was used, along with an AG11 guard column (50 mm × 2 mm). The separation was conducted under gradient conditions with potassium hydroxide. The gradient program was as follows: 0–2 min, 1.0 mM KOH; 2–5 min, 1.0–2.5 mM KOH; 5–12 min, 2.5–4.0 mM KOH; 12–16 min, 4.0 mM KOH; 16–17 min, 4.0–1.0 mM KOH. The flow rate was set at 0.25 ml/min.

Lipid extraction

Lipids were extracted from 20 μl of plasma using a modified version of the Bligh and Dyer's method, as previously described.[54] In brief, 750 μl of chloroform:methanol (1:2, v/v) was added to plasma samples and incubated at 1,500 rpm for 30 min at 4°C. After incubation, 350 μl of deionized water and 250 μl of chloroform were added to induce phase separation. The samples were then centrifuged, and the lower organic phase containing lipids was extracted into a clean tube. Lipid extraction was repeated once by adding 450 μl of chloroform to the remaining aqueous phase, and the lipid extracts were pooled into a single tube and dried in the SpeedVac under OH mode. Samples were stored at -80°C until further analysis.

Lipidome measurement and quantification

Lipidomic analyses were conducted at LipidALL Technologies using a Shimadzu Nexera 20-AD HPLC coupled with Sciex QTRAP 6500 PLUS as previously reported.[54] Separation of individual lipid classes of polar lipids by normal phase (NP)-HPLC was carried out using a TUP-HB silica column (i.d. 150×2.1 mm, 3 μm) with the following conditions: mobile phase A (chloroform: methanol:ammonium hydroxide, 89.5:10:0.5) and mobile phase B (chloroform:methanol:ammonium hydroxide:water, 55:39:0.5:5.5). MRM transitions were set up for comparative analysis of various polar lipids. Individual lipid species were quantified by referencing to spiked internal standards. D9-PC32:0(16:0/16:0), d9-PC36:1p(18:0p/18:1), d7-PE33:1(15:0/18:1), d9-PE36:1p(18:0p/18:1), d31-PS(d31-16:0/18:1), d7-PA33:1(15:0/18:1), d7-PG33:1(15:0/18:1), d7-PI33:1(15:0/18:1), C17-SL, C14-BMP, Cer d18:1/15:0-d7, d9-SM d18:1/18:1, C8-GluCer, C8-GalCer, d3-LacCer d18:1/16:0, Gb3 d18:1/17:0, d3-16:0 carnitine, d7-LPC18:1, d7-LPE18:1, C17-LPI,

C17-LPA, C17-LPS, C17-LPG, d17:1 Sph, d17:1 S1P were obtained from Avanti Polar Lipids. GM3-d18:1/18:0-d3 was purchased from Matreya LLC. Free fatty acids were quantitated using d31-16:0 (Sigma-Aldrich) and d8-20:4 (Cayman Chemicals).

Glycerol lipids including diacylglycerols (DAG) and triacylglycerols (TAG) were quantified using a modified version of reverse phase HPLC/MRM.[54] Separation of neutral lipids were achieved on a Phenomenex Kinetex-C18 column (i.d. 4.6×100 mm, 2.6 μm) using an isocratic mobile phase containing chloroform:methanol:0.1 M ammonium acetate 100:100:4 (v/v/v) at a flow rate of 300 μl for 10 min. Levels of short-, medium-, and long-chain TAGs were calculated by referencing to spiked internal standards of TAG(14:0)3-d5,TAG(16:0)3-d5 and TAG(18:0)3-d5 obtained from CDN isotopes, respectively. DAGs were quantified using d5-DAG17:0/17:0 and d5-DAG18:1/18:1 as internal standards (Avanti Polar Lipids).

Free cholesterols and cholesteryl esters were analyzed under atmospheric pressure chemical ionization (APCI) mode on a Jasper HPLC coupled to Sciex 4500 MD as described previously, using d6-cholesterol and d6-C18:0 cholesteryl ester (CE) (CDN isotopes) as internal standards.[54]

Lipid ontology enrichment and network analysis lipid ontology (LION) enrichment analysis was performed by inputting lipid lists into the LION/web online portal (http://www.lipidontology.com/), and then generating LION network view.[33]

Arteriography image acquisition, preprocessing, and time density curve (TDC) parameter calculation

Digital subtraction angiography (DSA) images were acquired using an Artis station (Siemens, Germany). Each DSA run was performed with a 4 ml/s injection of Vispaque (GE Healthcare Ireland Limited, Carrigtohill, Munster, Ireland) via an angiographic catheter positioned at the cervical segment of the internal carotid artery (ICA), with a total contrast volume of 6 ml.

The acquisition parameters for most DSA sequences were as follows: pixel spacing, 0.217 × 0.217 mm; median peak tube voltage, 81.2 kV (interquartile range [IQR]: 77.9–83.8 kV); window center, 2047; window width, 4095; cine rate, 4 frames per second; and median frames per DICOM file, 49 (IQR: 41–58).

For each DSA run, cerebral blood flow (CBF) and cerebral blood volume (CBV) were calculated from the TDC at each pixel. A simplified gamma variate function was used to fit the TDC, with image preprocessing and TDC fitting implemented in Python (version 3.6.1). CBV, serving as a relative index of blood flow volume, was determined by integrating the TDC over 10 sec. CBF was calculated by dividing the CBV by the mean transit time.

Magnetic resonance imaging data acquisition and brain volume analysis

Magnetic resonance imaging (MRI) scans were performed using a 3.0 T Trio Siemens scanner (Siemens, Erlangen, Germany). All subjects were secured with a belt and foam pads to minimize head movement, and headphones were used to reduce scanner noise. A rapid gradient-echo sequence was employed with three-dimensional magnetization to obtain high-resolution T1-weighted anatomical images. The imaging parameters were as follows: repetition time = 1900 ms, echo time = 2.48 ms, inversion time = 900 ms, flip angle = 9°, slices = 176, thickness = 1.0 mm, gap = 0 mm, matrix = 256 × 256, field of view = 250 mm × 250 mm, and number of excitations = 2. Image data preprocessing was performed using Voxel-Based Morphometry 8 (VBM8; http://dbm.neuro.uni-jena.de/vbm8/) within the Statistical Parametric Mapping 8 (SPM8) package (Institute of Neurology, London, U.K.) running under MATLAB (The MathWorks, Inc., Natick, MA). The anatomical images of all subjects were segmented into gray matter (GM), white matter (WM), and cerebrospinal fluid (CSF), and their volume values were recorded for subsequent analysis. Additionally, the sum of these volume values was calculated as the total brain volume for each subject for further analysis.

Stable isotope tracing of metabolites in mice

All animal studies were approved by the Institutional Animal Care and Use Committee at the Chinese Institute for Brain Research, Beijing. Male C57BL/6N mice were purchased from Charles River Laboratories. Tracer experiments were conducted on mice aged 8–12 weeks. A catheter (Instech, C20PV-MJV1301, 2 French, 10 cm) was implanted in the right jugular vein and connected to a vascular access button (Instech, VABM1B/25, 25 gauge, one-channel button). Mice were allowed to recover from surgery for at least one day and were fasted for 8 h before infusion.

[U-13C]Glucose (>99% purity, HY-B0389S10, MedChemExpress) was diluted to 715 mM in sterile water (not saline) and stored at 4 °C until the experiment. The infusion procedure included a priming bolus of 125 μl per mouse administered over 60 sec, followed by a continuous infusion at 2.5 μl/min per mouse for 2.5 h. Similarly, [U-13C]Glutamate (>99% purity, HY-14608S5, MedChemExpress) was diluted to 5.5 mM in sterile saline and stored at 4 °C until the experiment. The infusion procedure included a priming bolus of 150 μl per mouse over 10 min, followed by a continuous infusion at 2.5 μl/min per mouse for 2.5 h.

Blood samples were collected from the retro-orbital venous plexus before infusion and at 20, 50, 90, and 150 min after the start of infusion. Animals were euthanized by cervical dislocation, followed by rapid dissection of the brain and thigh muscles. Tissues were immediately snap-frozen in liquid nitrogen and stored at −80°C.

For blood samples, plasma was separated by centrifugation at 4 °C, 1000 g for 10 min. A 5 μl aliquot of plasma was extracted with 40 μl of 90% acetonitrile, centrifuged at 4 °C, 21,130 g for 15 min, and transferred to an MS vial for measurement. For brain and muscle tissue samples, snap-frozen tissues were kept on dry ice. A clean scalpel and forceps were used to cut small pieces of tissue. For every 10 mg of tissue, 80 μl of pure water was added, and the tissue was ground. Then, 320 μl of pure acetonitrile was added, and the tissue was further ground with a pestle until fully dissociated. The mixture was centrifuged at 21,130 g for 20 min at 4 °C to remove debris. A 200 μl aliquot of the supernatant was transferred to a new tube and dried into a powder using a SpeedVac. The dried

metabolites were stored at −80°C until mass spectrometry analysis. For analysis, the dried metabolites were reconstituted in 100 μl of 80% acetonitrile (5 mg tissue/100 μl) and injected into the mass spectrometer.

Statistical analysis and data visualization

We conducted unsupervised and supervised multivariate data analysis with principal component analysis (PCA), hierarchical clustering, and partial least squares discriminant analysis (PLS-DA). The following statistical procedures were used: normalization to the sum of peak areas of all ion features, $\log_{10}$ transformation, and auto-scaling. PCA, PLS-DA, metabolite set enrichment analysis and pathway analysis were carried out using MetaboAnalyst 5.0 (Montreal, QC, Canada).[11] For each patient's paired arteriovenous comparison, the peak area for all detected substances underwent normalization to the median of the arteriovenous ratio. This was achieved using the probabilistic quotient normalization method.[9,55,56] For each participant, we calculated the ratio of metabolite abundance in the vein (V) relative to the artery (A). Using a paired test to compare the abundance of these compounds in the artery and the vein, metabolites with *p*-values less than 0.05 were considered to exhibit significant net uptake or release. A median V/A ratio of less than 1 indicates net uptake, while a ratio greater than 1 indicates net release.

To compare data between the artery and vein of each patient, a paired *t*-test was used when the data exhibited a normal distribution ($p > 0.05$ by Shapiro-Wilk test). Otherwise, the Wilcoxon paired-samples signed rank test was used. To explore the impact of age on the absorption and release of metabolites in the brain, a Student's *t*-test was used to compare the arteriovenous ratios of each metabolite in the two populations. *P* values were adjusted for multiple comparisons using the Benjamini-Hochberg method, with a FDR cutoff of 0.05. The Shapiro-Wilk test, paired *t*-test, Wilcoxon paired-samples signed rank test, Student's *t*-test, and *p*-value correction were all conducted using R version 4.1.2 (Vienna, Austria). The generation of volcano plots, heatmaps, scatter plots, and donut charts was performed in R. Two-way ANOVA of interaction between disease subtype and age was performed in R.

Linear regression models of the plasma metabolome that included disease subtype, age, and their interaction term was built in R. Bar graphs were generated using GraphPad Prism software version 8.0.2 (GraphPad Software Inc., California, USA).

Neuron, Volume *113*

Supplemental information

Comprehensive characterization of metabolic consumption and production by the human brain

Yilong Wang, Lebo Zhou, Nan Wang, Baoshan Qiu, Di Yao, Jie Yu, Miaoqing He, Tong Li, Yufeng Xie, Xiaoqian Yu, Zhanying Bi, Xiangli Sun, Xunming Ji, Zhen Li, Dapeng Mo, and Woo-ping Ge

Supplemental information

Comprehensive characterization of metabolic consumption and production by the human brain

Yilong Wang, Lebo Zhou, Nan Wang, Baoshan Qiu, Di Yao, Jie Yu, Miaoqing He, Tong Li, Yufeng Xie , Xiaoqian Yu, Zhanying Bi, Xiangli Sun, Xunming Ji, Zhen Li, Dapeng Mo, Woo-ping Ge

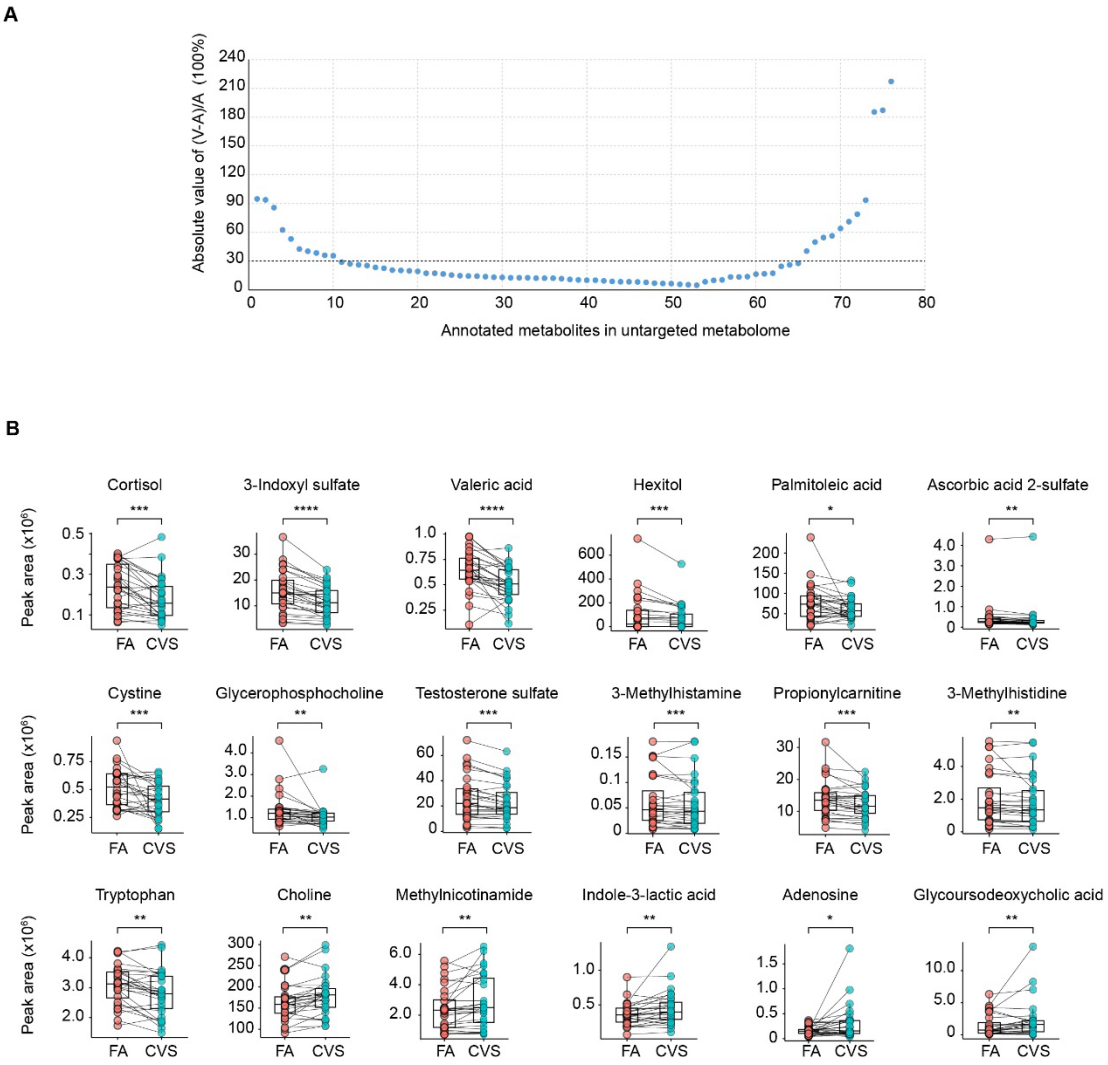

Figure S1. Metabolite uptake/release ratios in the untargeted metabolome, related to Figure 1.

A. The uptake/release ratios of annotated metabolites in the untargeted metabolome of the brain from plasma samples. Among these metabolites, 55 of 76 have ratios <30%.

B. Paired scatter plots with connecting lines representing the arterial and venous comparison of representative metabolites. Box plots depict median and lower and upper quartiles. Significance determined using p-values after a two-tailed paired t-test or one-sample Wilcoxon test. *$p < 0.05$, **$p < 0.01$, ***$p < 0.001$, ****$p < 0.0001$.

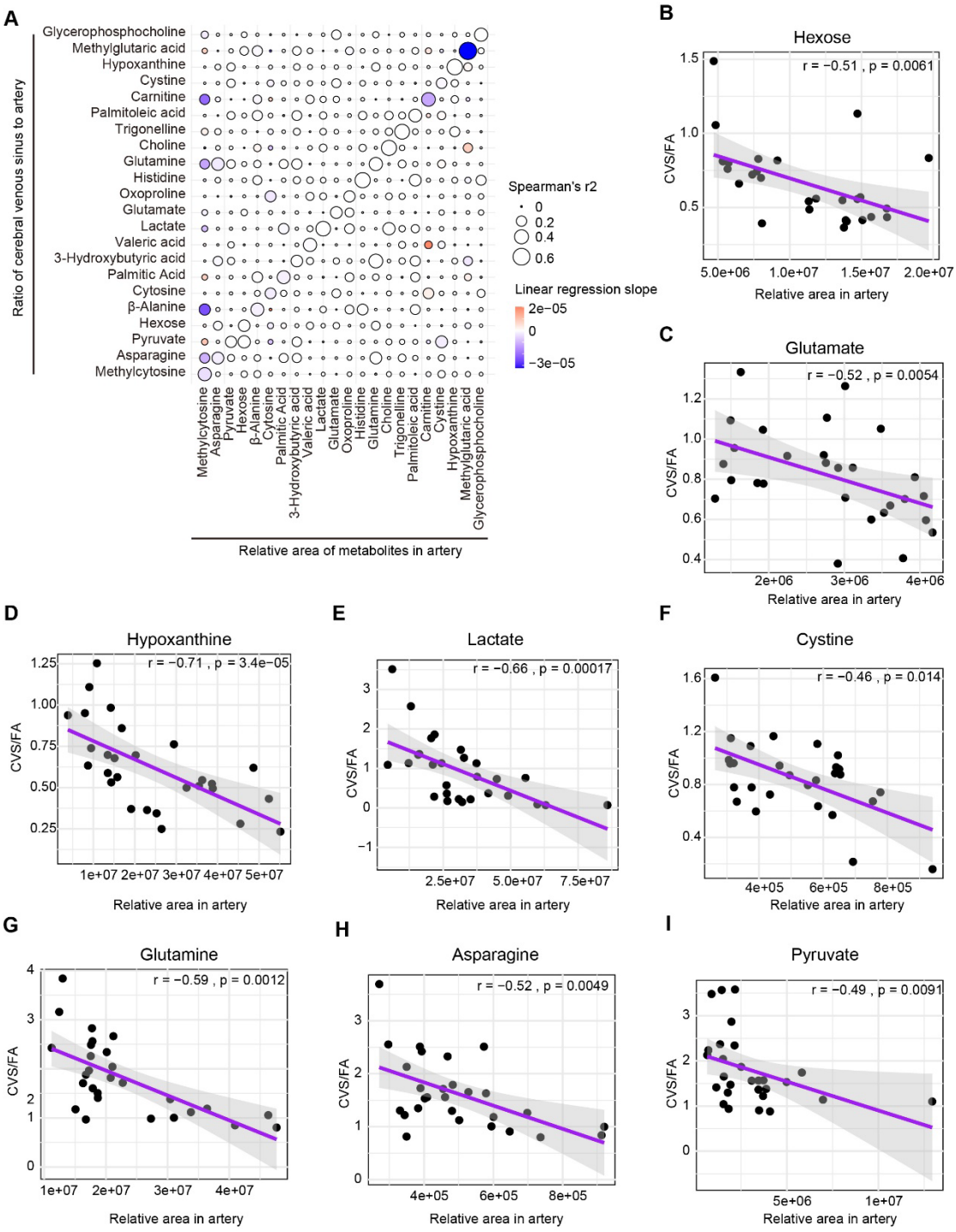

Figure S2. Brain uptake and release of representative metabolites primarily depends upon circulating levels, related to Figure 1 and Figure 2.

A. Relationship between CVS-to-artery ratio (CVS/FA) and arterial level of indicated metabolites, as evaluated by Spearman's correlation test and linear regression.

B–I. Artery levels versus uptake/release of indicated metabolites by the brain. P value and r were generated by Spearman's correlation test.

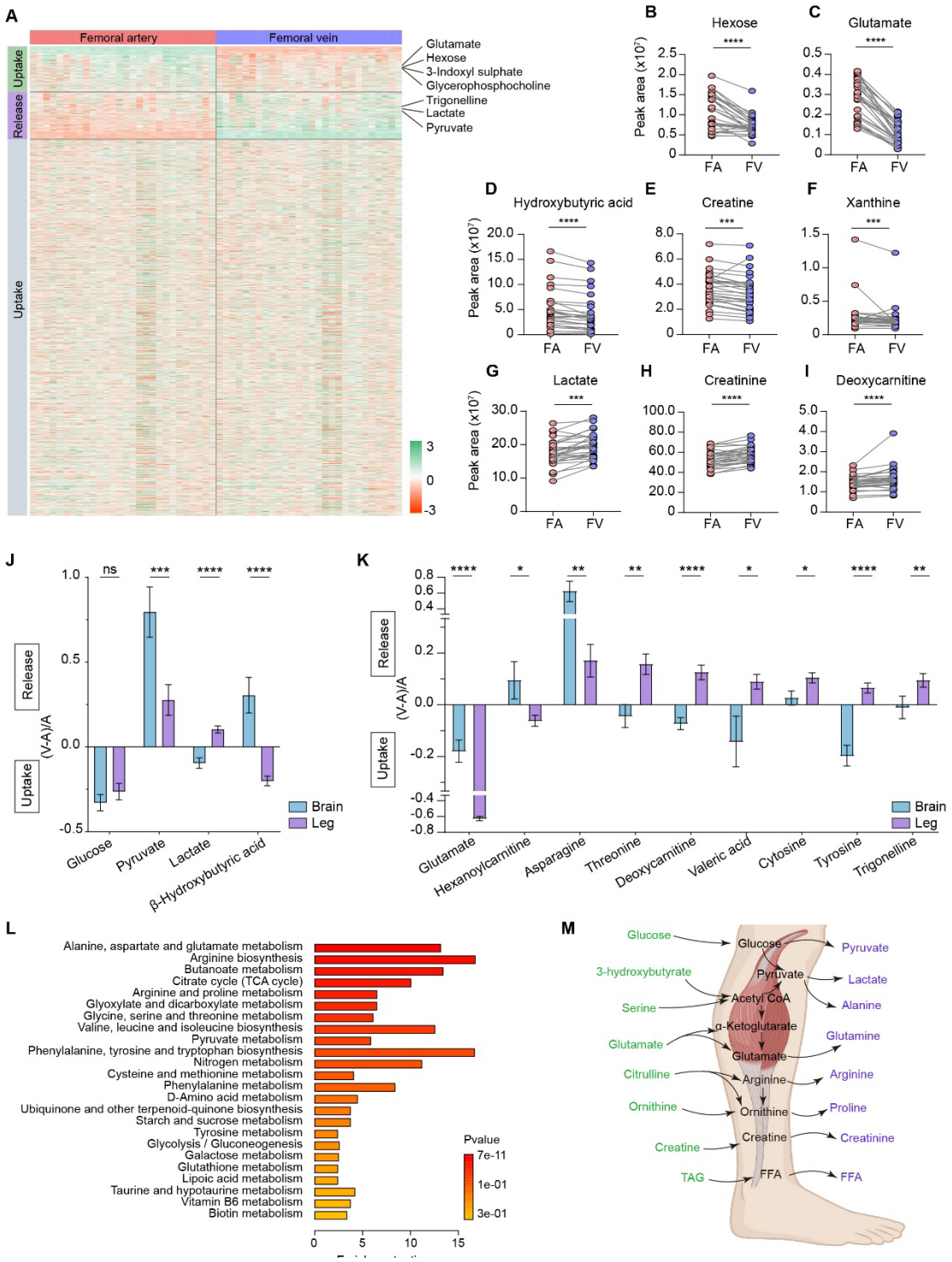

Figure S3. Characterization and pathway analysis of representative leg metabolites, related to Figure 1.

A. Heatmap showing relative abundance of detected compounds in plasma from the femoral artery and femoral vein for the 28 participants. Scale bar indicates relative abundance.

B–I. Scatter plots display the peak areas of metabolites, including hexose (B), glutamate (C), β-hydroxybutyric acid (D), creatine (E), xanthine (F), lactate (G), creatinine (H), and deoxycarnitine (I) in femoral artery (FA) and femoral vein (FV) samples. Lines connecting two data points indicate samples from the same individual. Significance was assessed using Benjamini-Hochberg–corrected *p*-values after two-tailed paired *t*-tests or one-sample Wilcoxon tests.

J. Comparison of the uptake and release ratios of glucose, pyruvate, lactate, and β-hydroxybutyric acid for the brain and leg.

K. Comparison of the uptake and release ratios of glutamate, hexanoylcarnitine, asparagine, threonine, deoxycarnitine, valeric acid, cytosine, tyrosine, and trigonelline for the brain and leg. Data are shown as the mean ± standard error. Significance assessed by two-tailed *t*-test. *$p < 0.05$, **$p < 0.01$, ***$p < 0.001$, ****$p < 0.0001$; ns, not significant.

L. Metabolite set enrichment analysis (MSEA) for metabolites taken up by the human leg, featuring the top 24 pathways.

M. Summary diagram of representative pathways related to energy metabolism, including glucose metabolism, various amino acid metabolism pathways, and lipolysis.

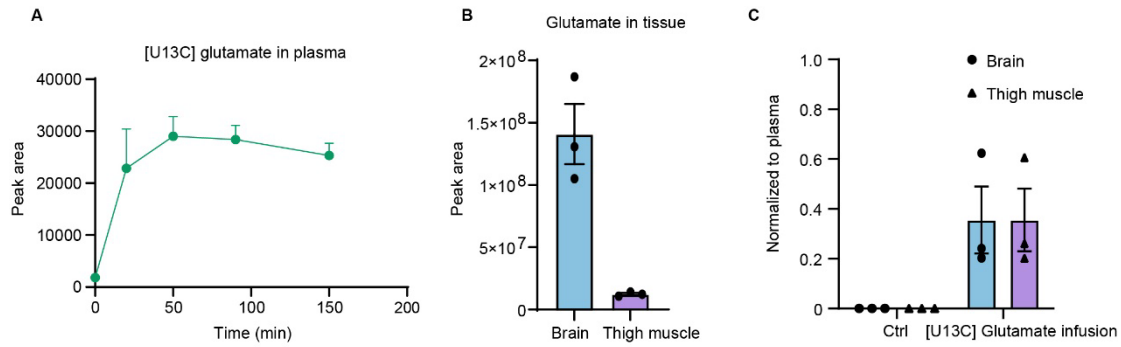

Figure S4. In vivo measurement of glutamate by kinetic [U13C] glutamate infusion, related to Figure 2.

A. Time course of plasma [U13C] glutamate and [U13C] glutamine enrichment during [U13C] glutamate infusion in mice.

B. Relative glutamate levels in the brain and thigh muscle(n = 3 mice).

C. Average carbon atom labeling of glutamate normalized to plasma in the mouse brain after [U13C] glutamate infusion and in ctrl mice. n = 3 mice for each group. The average carbon atom labeling was calculated using the formula $[\sum_{i=0}^{n}(Mi \cdot i)]$/n where n = 5 as glutamate has five carbons, and Mi is the ratio of glutamate's M + i form, normalized to the average carbon atom labeling of the infused tracer in plasma.

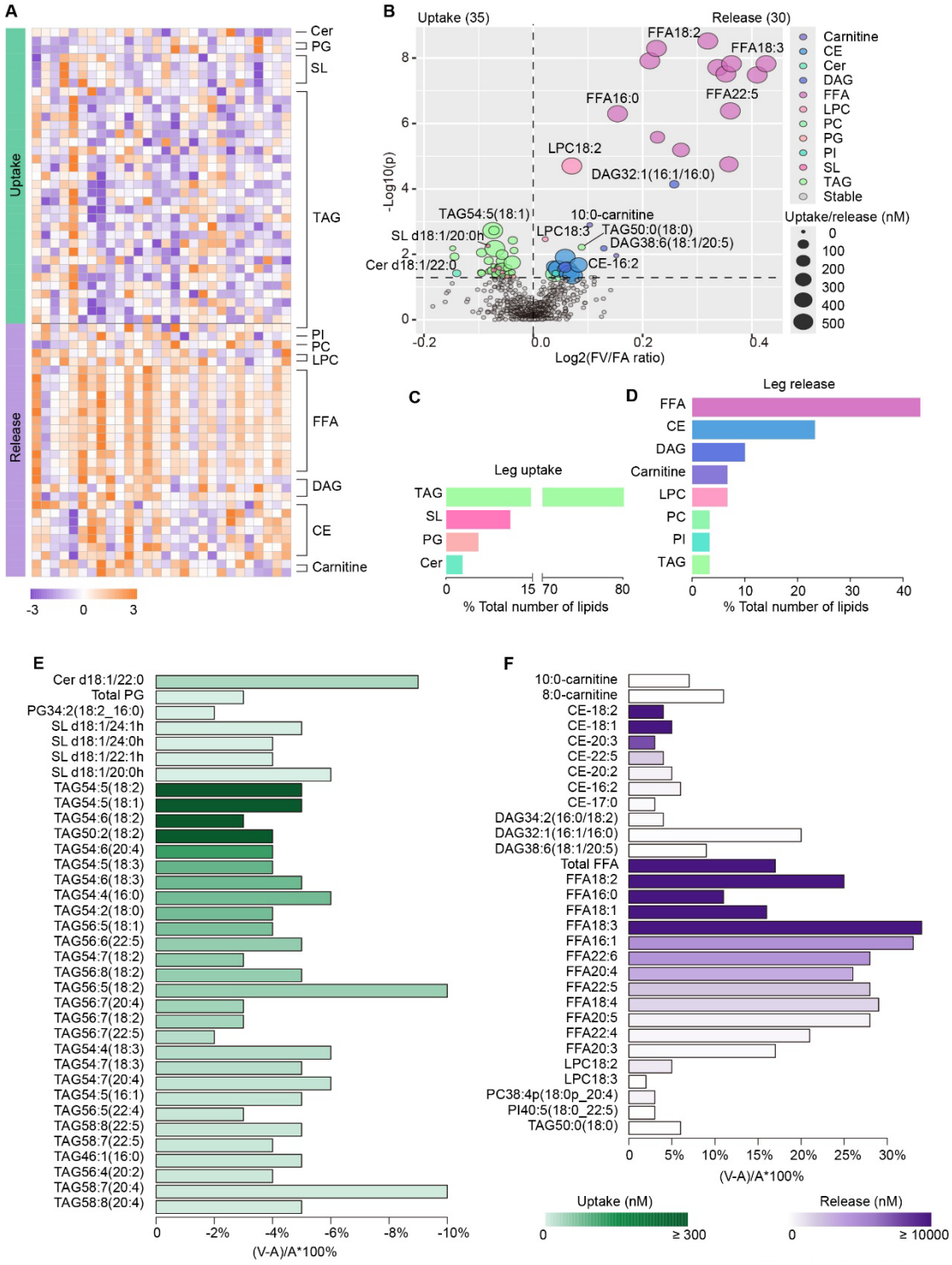

Figure S5. Lipid uptake and release by the human leg, related to Figure 4 and Figure 5.

A. Heatmap showing differences of lipid abundance in FV versus FA. Scale bar indicates relative lipid differences in FV versus FA.

B. Volcano plot showing lipids taken up by and released from the human brain.

Significant FA - FV differences in the leg were determined using two-tailed paired *t*-tests or one-sample Wilcoxon tests. Vertical dashed line indicates $p = 0.05$; horizontal dashed line indicates no A-V difference, i.e., $\log_2(FV/FA) = 0$.

C. Class composition of lipids taken up by the leg. Number of lipids in each lipid class as a

percentage of the total number of lipids taken up by the leg.

D. Class composition of lipids released by the leg. Number of lipids in each lipid class as a

percentage of the total number of lipids released by the leg.

E, F.) The net uptake (E) and release (F) in nanomoles per liter of blood flowing through the leg and the ratios of lipids consumed by the human leg.

Bar colors denote lipid uptake or release, whereas the intensity of the shading reflects the absolute quantities of net uptake or release. The lengths of the bars represent the uptake (E) or release (F) ratios of the corresponding lipids.

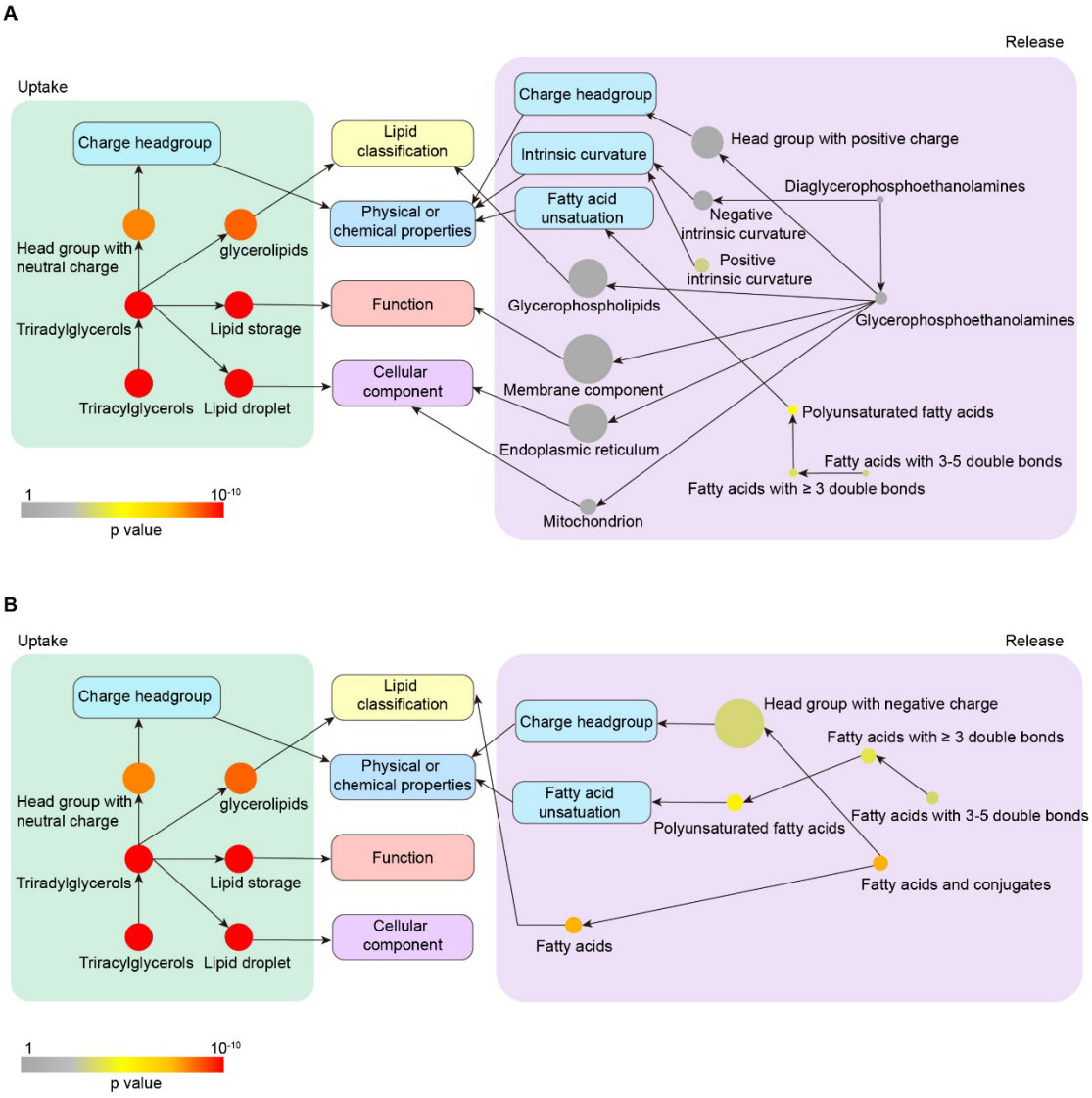

Figure S6. The network view of LION-term enrichment analysis of lipids taken up or released by brain or leg, related to Figures 4 and 5.

A. The network view of LION-term enrichment analysis of lipids taken up or released by brain.

B. The network view of LION-term enrichment analysis of lipids taken up or released by leg. Dot sizes in the plots are scaled to the number of associated lipids; colors are scaled to the level of enrichment (*p* values).

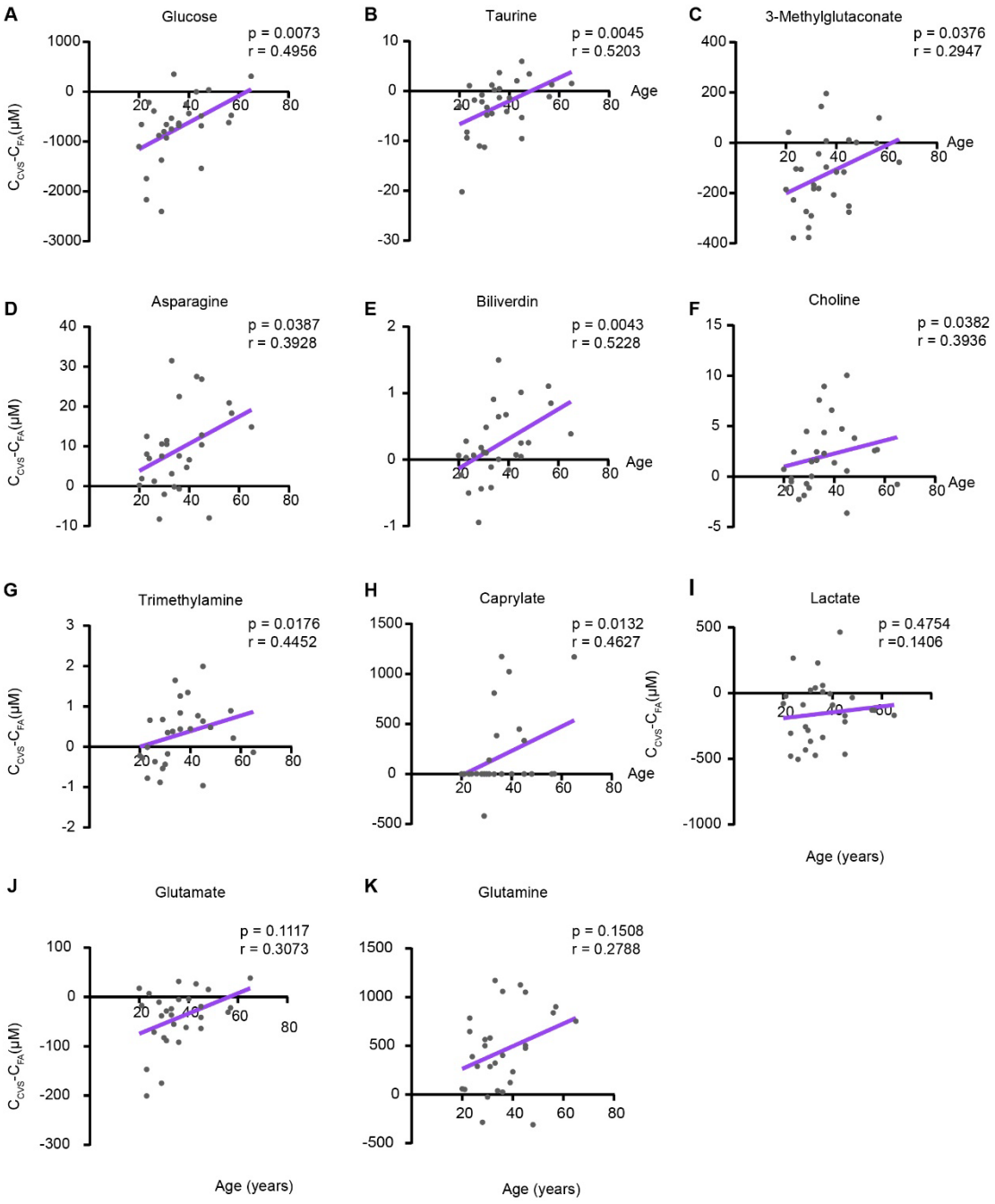

Figure S7. Relationship between brain uptake and release of representative metabolites with age, related to Figure 6.

A–K. Correlation analysis of CVS-FA gradient (μM) of representative metabolites with age by linear regression. *P*-values and r-values were generated by Spearman's correlation test.

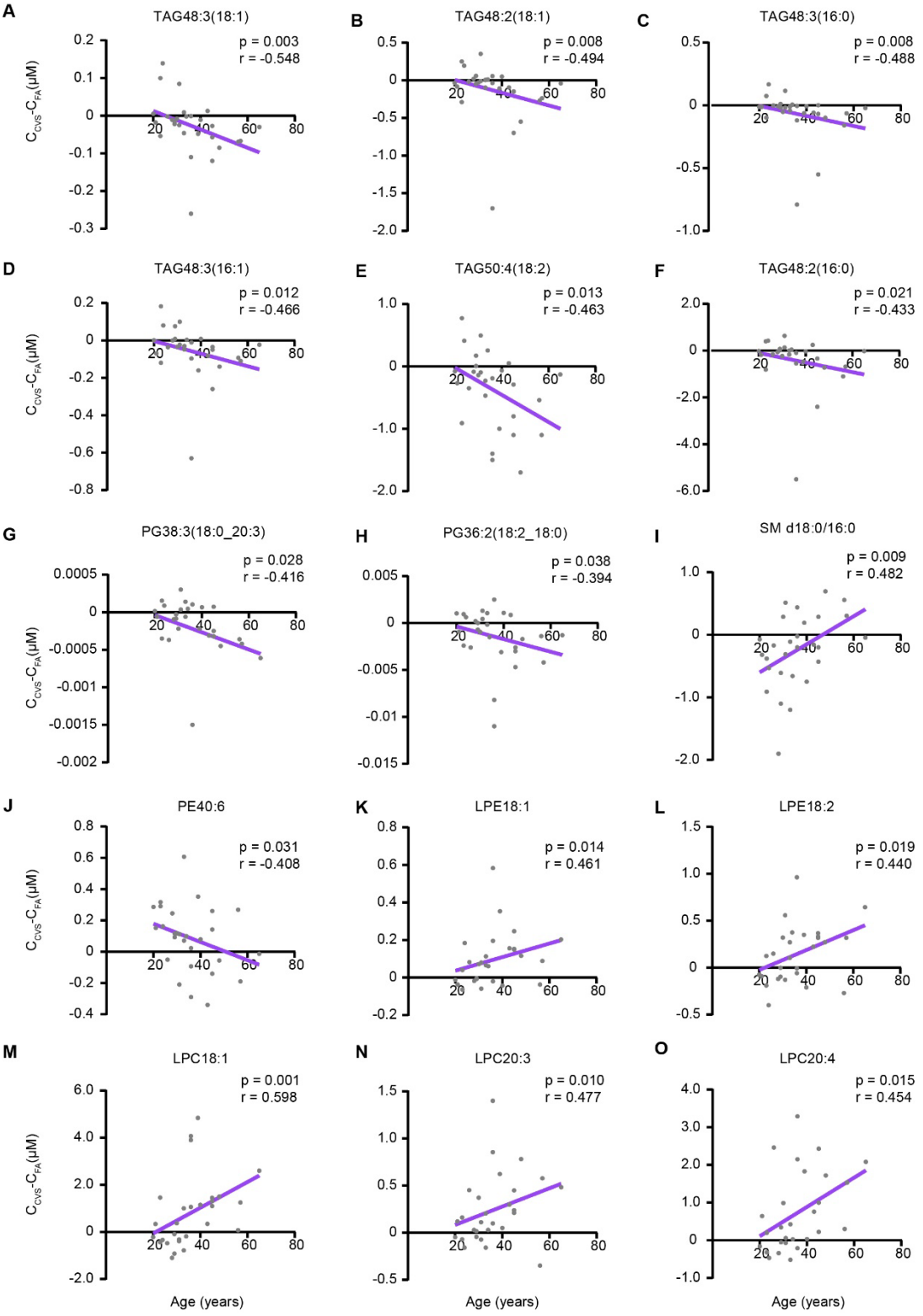

Figure S8. Relationship between brain uptake and release of representative lipids with age, related to Figure 6.

A–O. Correlation analysis of CVS-FA gradient (μM) of lipids with age by linear regression. *P* value and r were generated by spearman correlation test.

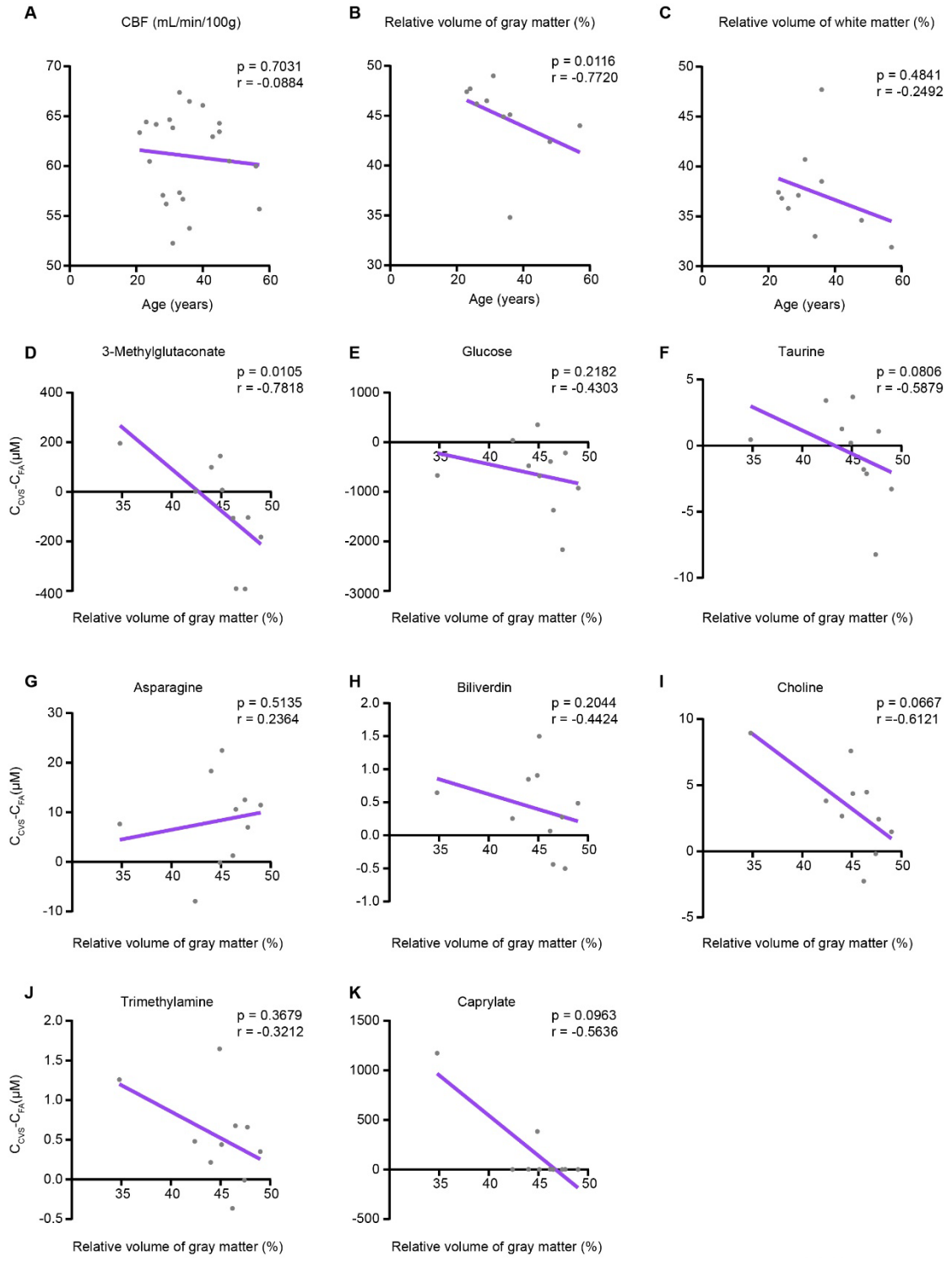

Figure S9. Relationship between cerebral blood flow and brain volume with age, and the relationship between brain uptake and release of representative metabolites with brain volume, related to Figure 6.

A–C. Correlation analyses of cerebral blood flow (CBF), relative volume of gray matter (%), and relative volume of white matter (%) with age, using linear regression.

D–K. Correlation analysis of the CVS-FA gradients (μM) of metabolites with the relative volume of white matter (%), using linear regression. P-values and r-values were generated by Spearman's correlation test.

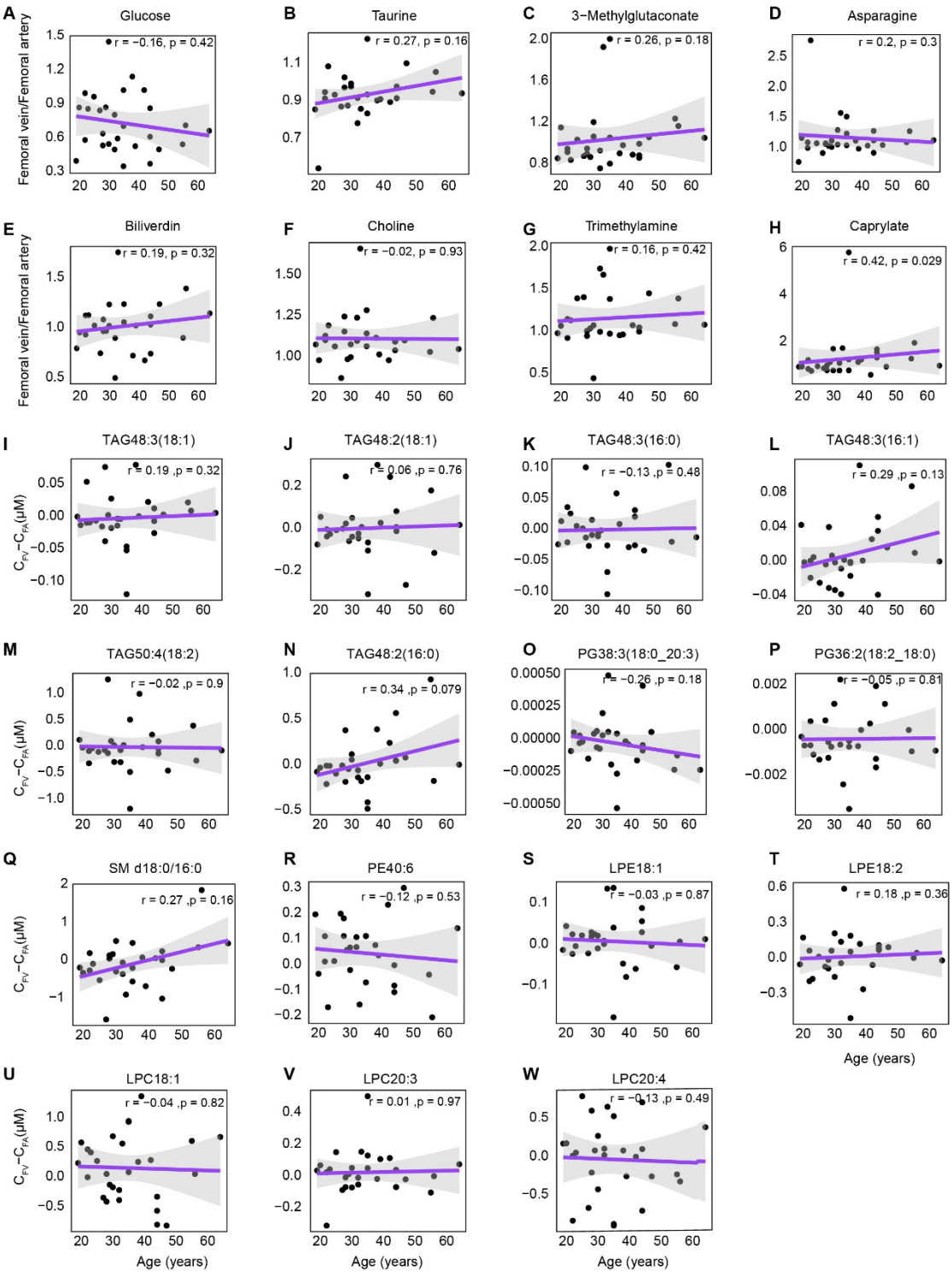

Figure S10. Relationship between age and the uptake and release of representative metabolites and lipids in the legs, related to Figure 6.

A–W. Correlation analysis of FV-FA gradient (μM) of metabolites and lipids with age by linear regression. *P* value and r were generated by Spearman's correlation test.